Accepted Manuscript

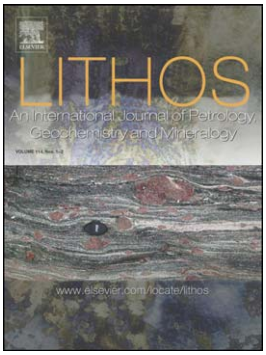

The Cotoncello Shear Zone (Elba Island, Italy): The deep root of a fossil oceanic detachment fault in the Ligurian ophiolites

Chiara Frassi, Giovanni Musumeci, Michele Zucali, Francesco Mazzarini, Gisella Rebay, Antonio Langone

PII: S0024-4937(17)30071-3
DOI: doi:10.1016/j.lithos.2017.02.015
Reference: LITHOS 4244

To appear in: *LITHOS*

Received date: 28 October 2016
Accepted date: 18 February 2017

Please cite this article as: Frassi, Chiara, Musumeci, Giovanni, Zucali, Michele, Mazzarini, Francesco, Rebay, Gisella, Langone, Antonio, The Cotoncello Shear Zone (Elba Island, Italy): The deep root of a fossil oceanic detachment fault in the Ligurian ophiolites, *LITHOS* (2017), doi:10.1016/j.lithos.2017.02.015

This is a PDF file of an unedited manuscript that has been accepted for publication. As a service to our customers we are providing this early version of the manuscript. The manuscript will undergo copyediting, typesetting, and review of the resulting proof before it is published in its final form. Please note that during the production process errors may be discovered which could affect the content, and all legal disclaimers that apply to the journal pertain.

ACCEPTED MANUSCRIPT

The Cotoncello Shear Zone (Elba Island, Italy): the deep root of a fossil oceanic detachment fault in the Ligurian ophiolites

Chiara Frassi[1,*], Giovanni Musumeci[1], Michele Zucali[2], Francesco Mazzarini[3], Gisella Rebay[4] and Antonio Langone[5]

[1] Dipartimento di Scienze della Terra, Università di Pisa, Via S. Maria, 53, 56126 Pisa, Italy.

[2] Dipartimento di Scienze della Terra, Università degli Studi di Milano, Via Mangiagalli, 34, 20133 Milano, Italy.

[3] Istituto Nazionale di Geofisica e Vulcanologia, Sezione di Pisa, Via della Faggiola 32, 56126 Pisa, Italy.

[4] Dipartimento di Scienze della Terra e dell'Ambiente, Università degli studi di Pavia, Via Ferrata, 1, Pavia, Italy.

[5] Istituto di Geoscienze e Georisorse, CNR, Via U.O.S. of Pavia, via Ferrata, 1, Pavia, Italy.

[*] Corresponding author. E-mail: chiarafrassi@gmail.com

ACCEPTED MANUSCRIPT

Abstract

The ophiolite sequences in the western Elba Island are classically interpreted as a well-exposed ocean-floor section emplaced during the Apennines orogeny at the top of the tectonic nappe-stack. Stratigraphic association along with petrographic and geochemical features indicate that these

ACCEPTED MANUSCRIPT

ophiolite sequences are remnants of slow- ultraslow spreading oceanic lithosphere analogous to the present-day Mid-Atlantic Ridge and Southwest Indian Ridge.

Within the oceanward section of Tethyan lithosphere exposed in the Elba Island, we investigated for the first time a decameter-thick structure, the Cotoncello Shear Zone (CSZ), that records high-temperature ductile deformation. We used a multidisciplinary approach to document the tectono-metamorphic evolution of the shear zone and its role during spreading of the western Tethys. In addition, we used zircon U-Pb ages to date formation of the gabbroic lower crust in this sector of the Apennines. Our results indicate that the CSZ rooted below the brittle-ductile transition at temperature above 800 °C. An high-temperature ductile fabric was overprinted by fabrics recorded during progressive exhumation up to shallower levers under temperature < 500°C. We suggest that the CSZ may represent the deep root of a detachment fault that accomplished exhumation of an ancient oceanic core complex (OCC) in between two stages of magmatic accretion. We suggest that the CSZ represents an excellent on-land example enabling to assess relationships between magmatism and deformation when extensional oceanic detachments are at work.

Keywords: Oceanic core complexes, Slow-spreading ridge, brittle-plastic transition, Northern Apennines ophiolites, Elba island.

1. Introduction

In slow- and ultraslow-spreading ridges (plate motion < 5 cm/year) the generation of new oceanic lithosphere is strongly controlled by the activity of detachment faults that accomplish exhumation of 150-6000 km^2 wide portions of lower- crust gabbros and mantle rocks (Oceanic Core Complex, OCC; MacLeod et al., 2002, 2009; Ohara et al., 2003; Escartin et al., 2008). In the

ACCEPTED MANUSCRIPT

last decades, bathymetric and geophysical studies associated to drill hole investigations and numerical simulations led to document sufficiently the active dynamic processes and the rock assemblages and composition of lower crust/mantle sections exposed at the OCC surface. In modern OCCs (Harigane et al., 2008; MacLeod et al., 2009; Hansen et al., 2013), detachment faults typically associate to ophiolite breccias unconformably overlying gabbros and mantle basement that contains hydrous alteration phases formed as the result of fluid-rock interaction (serpentine, talc, chlorite; Cann et al., 1997; Tucholke et al., 1998; Boschi et al., 2006; Karson et al., 2006; MacLeod et al., 2009). Although the evolution of lower crust-mantle sections exhumed in oceanic core complexes are intensively studied, many uncertainties still concern the dynamics of oceanic detachments and the rheology of the deep oceanic crust. The inability to investigate these structures "in the field", in fact, makes very difficult gathering information on: (1) the spatial and temporal localization of deformation along the oceanic detachment fault, (2) the mechanism, rheology and the deep extent of the detachment and (3) how tectonics, magmatism and hydrothermal processes enhance the strain localization during the OCCs evolution.

Important information that could help addressing these questions may be acquired by studies of fossil OCCs exposed on land. In the last decades, in fact, detailed field mapping associated with structural, stratigraphic, petrographic and geochemical studies enabled reconstructing the geometry and the internal structure of fossil OCCs, the stratigraphy of supradetachment sequences and the spatial and temporal relations between geometry, magmatism and tectonics at shallow level (Tremblay et al., 2009; Manatschal et al., 2011; Balestro et al., 2015; Festa et al., 2015; Lagabrielle et al., 2015; Nicholas et al., 2017).

On the contrary, the deep roots of the OCCs are scarcely investigated. In the modern and in exhumed analogues OCCs, in fact, few works document the presence of a pervasive high-temperature viscous deformation broadly associated to the oceanic detachment fault developed below the brittle-plastic transition (Molli, 1996; Miranda and Jones, 2010; Hanson et al., 2013;

ACCEPTED MANUSCRIPT

Manatschal et al., 2011; Nicholas et al., 2017). Consequently, further investigations are required to rheologically constrain the deep extension of the oceanic detachment fault.

In this study, we present field and microstructural descriptions and the results of lattice preferred orientation studies conducted on olivine and on amphibole from a previously unknown hundred-metre thick mylonite zone (Cotoncello Shear Zone) affecting the oceanic Tethyan lithosphere now exposed in western Elba Island (northern Apennine, Italy). Analogously to what documented in the modern Kane OCC, in the Mid-Atlantic Ridge (MAR) by Hansen et al., (2005), we describe structures that indicate a progressive shearing under retrogressive conditions that evolved from high-temperature viscous deformation to brittle-ductile localized shear zone. The CSZ preserves evidences that may help to understand the mechanism and the rheology of the deep extent of the oceanic detachment faults in modern OCC.

2. Tethyan ophiolite sequences in Northern Apennines

The ophiolite sequences in northern Apennines (Fig. 1) testify the Mesozoic evolution, from rifting to slow/ultraslow seafloor spreading, of the Tethys oceanic basin that, since Jurassic, separated the Adria and European continental plates (i.e. the Ligure-Piemontese Ocean). The knowledge of the primary architecture of the oceanic basin (Cortesogno et al., 1994 and references therein; Marroni and Pandolfi, 2007 and references therein) as well as the thermo-mechanical history of the oceanic lithosphere during mantle upwelling, lithosphere delamination and spreading (Molli, 1996; Tribuzio et al., 2000, 2004; 2015; Sanfilippo and Tribuzio, 2011; Piccardo et al., 2014 and references therein) have improved significantly during the last decades, discriminating ophiolites produced in a slow/ultraslow spreading setting (belonging to the Internal Ligurian Units) and ophiolites originated in an embryonic ridge environment and associated to continental lithospheric rocks (belonging to the External Ligurian Units) (Fig. 1). The Internal Ligurian Units represent the typical section of the Middle to Late Jurassic Tethyan oceanic lithosphere. The

ACCEPTED MANUSCRIPT

lithosphere sequence is less than 1 km thick and consists of depleted-mantle peridotite (Piccardo et al., 2014 and references therein) intruded by small amounts of MOR-type gabbroic complexes. The peridotite-gabbro association is covered by a Late Jurassic-Paleocene volcano-sedimentary complex in which sedimentary breccias, MORB-type basalt flows and radiolarian cherts are mutually interlayered (Marroni and Pandolfi, 2007 and references therein). Structures, rock assemblages and compositions indicate that this lithosphere sequence is analogous to what produced in the present-day slow/ultraslow spreading setting along the Mid Atlantic Ridge (e.g. Marroni et al., 2010 and references therein; Sanfilippo and Tribuzio, 2011). On the contrary, in the External Ligurian Units, ophiolites preserve evidences of an ocean-continent transitional domain. In these units, ophiolites occur as huge slide-blocks of fertile sub-continental lithosphere Sp-lerzholites, gabbros and basalts (retaining primary contact relationships with lower and late Permian continental crust) in late Cretaceous sedimentary mélanges (Marroni et al., 2001 and references therein) (Fig. 1). During their Oligo-Miocene emplacement on the top of the northern Apennine nappe stack, the ophiolite sequences experienced a polyphase deformation history and prehnite-pumpellyite to blueschists facies metamorphic conditions (Marroni et al., 2010 and references therein).

2.1. Pre-orogenic deformation and metamorphism in the Northern Apenninic ophiolites

Mylonite fabrics have been documented in gabbros and peridotites from both the Internal (e.g. Cortesogno et al., 1994 and references therein; Molli, 1996 with references therein) and the External (e.g. Molli, 1996; Tribuzio et al., 2014) Ligurian Units. Most of these shear zones have been described in gabbroic rocks, whereas very few studies have provided a structural and metamorphic description of mylonite fabrics in peridotites (e.g. Molli, 1996). Even though peridotite tectonites have been recognised in several places in the Northern Apennines, their microstructures and their pressure and temperature stability field are poorly investigated.

Mafic and ultramafic mylonitic rocks preserved within slide blocks in the External Ligurian

ACCEPTED MANUSCRIPT

Units provide structural and metamorphic information about the Late Triassic mantle upwelling (e.g. Montanini et al., 2012) and transition from continental breakup to slow-seafloor spreading. Granular fabric in spinel peridotite was constrained at T = 1000-1300 °C (Tribuzio et al., 2004) whereas later recrystallization of orthopyroxene occurred at lower temperature (T = 900-1040 °C, P = 1.5G Pa: Tribuzio et al., 2004). In gabbros, clinopyroxene + plagioclase-bearing mylonites developed probably close to sub-solidus conditions at T ~ 850 °C with no involvement of seawater (Tribuzio et al., 2014). Mylonitic gabbros successively develop an amphibole-bearing foliation at ~ 710 °C (Tribuzio et al., 2014). Recent U-Pb zircon geochronology constrains the formation of lower gabbroic crust during the incipient oceanic lithosphere at ~161-173 (Ma Tribuzio et al., 2004; 2016).

Peridotites from the Internal Ligurian Units (Fig. 1) recorded an early shearing event (Molli, 1996) occurred probably before their re-equilibration in the plagioclase stability field (T = 900-1000 °C and P = 0.5 – 0.7 GPa; Rampone et al., 1993). After the Middle Jurassic gabbro intrusions around 161-163 Ma (Tribuzio et al., 2016) at less than 15-20 km of depth (Tribuzio et al., 1995), the mafic and ultramafic complexes have been deformed by a long-lived shear zone developed under granulite/upper amphibolite facies conditions (T = 700 – 800 °C and P = 0.4 – 0.5 GPa: Molli, 1996; T = 660-730 °C and P = 0.3-0.4 GPa: Cortesogno et al., 1994) to greenschist facies conditions, that was responsible of the uplift of lower crust/mantle sections (Molli, 1996). At shallow structural levels, the increase in water content and the decrease in temperature (up to T ~ 550 °C: Cortesogno et al., 1994), lead to the growth of serpentine along mylonitic foliations in peridotites and contemporaneously Mg- hornblende / actinolite + plagioclase developed along the mylonitic foliation in gabbros (Molli, 1996 and references therein). Gabbros and peridotites were intensely fractured and locally affected by hydrothermal circulation that produced hornblende veining and coronae (Tribuzio et al., 2014) and intruded by basalt dykes (Cortesogno et al. 1994; Tribuzio et al., 2014). Shear zones, developed mainly at the gabbro/peridotite boundary (Cortesogno et al., 1994), were probably responsible of the final uplift and exposure at the seafloor.

ACCEPTED MANUSCRIPT

Intense hydrothermal circulation may occur through those late localized shear zones, inducing metasomatism and, at shallower levels, the development of calcite veins (Tribuzio et al., 2014) and/or ophicalcites (Cortesogno et al., 1994).

3. The geology of Elba Island

Located in the northern Tyrrhenian Sea (Fig. 1), the Elba Island consists of metamorphic and non-metamorphic units derived from both continental (i.e. the Tuscan) and oceanic (i.e. Ligurian) domains (Fig. 2) staked toward NE during the Oligocene - Miocene Apennines orogeny (Massa et al., 2016 and references therein). Analogously to the architecture described in Northern Apennines, the oceanic units exposed in the Elba Island are in the uppermost portions of the tectonic stack (Fig. 2). Late Cretaceous and middle Eocene to Paleocene carbonatic turbidites (i.e. External Ligurian Units; Raggi et al., 1965; Keller and Pialli, 1990) overthrusted tectonically the Tethyan oceanic sequence belonging to the Internal Ligurian Units (Fig. 2).

After the building of the Northern Apennines belt, a great variety of acid magmatic products including felsic laccoliths and two large plutons (Mt Capanne and Porto Azzurro plutons) intruded the tectonic nappe stack (c. 8 - 6.3 Ma: Dini et al., 2002; Barboni and Schoene, 2014 and references therein). Their emplacement locally produced low-pressure contact metamorphism (Barberi and Innocenti, 1965, 1966) that reached T ~600°C and P ~0.15–0.20 GPa (Rossetti et al., 2007). Close to the contact with igneous rocks (few teens of metres), serpentinized peridotites have olivine neoblasts and mm-sized anthophyllite crystals statically grown on original (and partly preserved) serpentine mesh structure (e.g. S.Ilario area; Fig. 1). The Mesozoic carbonatic host rocks record the static growth of wollastonite, grossular and Ca-pyroxene crystals, while andalusite, cordierite, plagioclase, actinolite and biotite develop in the late Jurassic cherts (Barberi and Innocenti, 1965; 1966). The intrusion of the Monte Capanne pluton at the core of a km- scale antiform, led to the centrifuge tilting of host rocks (Bouillin, 1983). The local stress field in the host rocks all around

ACCEPTED MANUSCRIPT

the pluton led to the development of centimeter to decimeter sized asymmetrical folds with axial planes dipping gently away from the pluton (Bouillin, 1983) and to ductile mylonites produced under submagmatic flow conditions in the porphyritic rocks intruded slightly earlier than the pluton emplacement (Westerman et al., 2004).

The knowledge of the gabbroic and mantle sequences exposed in the Elba Island is scarce also due to the HT-LP metamorphic overprint associated to the Mt. Capanne pluton. Geochemical and petrographical studies were conducted mainly in the eastern portion of the island (e.g. Bortolotti et al., 1994; Tartarotti and Vaggelli, 1994; Saccani and Principi, 2016), and only few studies investigated their tectono-metamorphic collisional evolution (Perrin, 1975; Reutter and Spohn, 1982). Little is known about their pre-orogenic history. Most of the studies agree that the oceanic lithosphere sequences cropping out in western Elba Island belong to the Internal Ligurian Units (e.g. Bortolotti et al., 1994; Saccani and Principi, 2016) and recorded a more complex and penetrative deformation compared to that documented in the ophiolite sequences of the eastern portion of the Elba island, but their involvement in the Apenninic orogenic prism and their tectono-metamorphic evolution during the Apenninic orogeny is still poorly constrained and with controversies. Most of the studies suggest that the ophiolites derive from the Penninic Units of western Alps (i.e. eastern Corsica Alpine belt) displaced eastward during the Apenninic orogeny through brittle-ductile shear zones and affected by meter-scale west-verging folds and by very low-grade metamorphism (e.g. Perrin, 1975). On the contrary Reutter and Spohn (1982) found low-grade metamorphic assemblages relicts (albite, chlorite, epidote and garnet) and east-verging structures, suggesting that the ophiolites may represent remains of an oceanic basin subducted westward during the Oligocene and then implicated in the late Oligocene-early Miocene northern Apennine stacking.

4. Methods

ACCEPTED MANUSCRIPT

The study of the CSZ involved a detailed structural description of lithologies and mesostructures summarised in Fig. 3. 35 samples were selected to be investigated using polarized light microscopy and scanning electron microscopy (SEM) located at the INGV in Pisa, in thin sections cut parallel to the mineral lineation and orthogonal to the main foliation. Two selected samples were analysed by X-rays powder diffraction (XRPD) to determine the composition of the mineralizations filling the late vein systems. Three samples representative of the main fabrics documented in peridotites were analysed to determine the lattice preferred orientation (LPO) of olivine and amphibole using a neutron diffraction texture analysis, or Quantitative Texture Analysis (QTA), at the nuclear reactor at the Institute Laue-Langevin in Grenoble, France. To constrain the age of mafic intrusion, U–Pb geochronology was carried out on zircons directly on polished thin section of one sample of deformed plagiogranite at the CNR – IGG of Pavia with Laser Ablation (LA)–ICP–MS. See Appendix for further methodological details.

5. The Cotoncello Shear Zone

The Cotoncello Shear Zone (CSZ) is exposed in the lower crust/mantle section cropping out along a vertical cliff in the northern margin of the Mt. Capanne pluton at ~500 m east of Punta del Cotoncello (western Elba Island) (Fig. 2). Though Miocene granitic porphyries (Portoferraio porphyry) limit on the west and on the east the shear zone (Fig. 3), the extremely continuous exposure along the seacoast (~150 m) makes the CSZ the widest section of sheared peridotites in northern Apennines. As described in the following sections, no evidence of low- to very low metamorphism or of the presence of deformative structures aquired during the Apennines orogeny are documented in the CSZ.

5.1. Geometry and structures at the outcrop scale

ACCEPTED MANUSCRIPT

The exposed rocks are mainly peridotite (~75%vol), gabbro (~22%), pyroxenite (~2%) and serpentinite (1%). Gabbro intrusions (5 to 15 m thick) are located in the central and westernmost portions of the CSZ whereas pyroxenites crop out as meter thick layers in the central and eastern portions (Fig. 3). Serpentinites occur exclusively in the eastern portion of the sheared basement. Gabbroic intrusions are cut by decimeter -thick foliated plagiogranite veins and by meter-thick undeformed basaltic dikes.

Several deformation fabrics, varying from proto-tectonite to mylonite-ultramylonite, were distinguished in the field (Figs. 3 and 4). All fabrics result parallel or sub-parallel to the different lithotypes (Fig. 3). The main foliation strikes NW-SE with an average direction of N130E and steeply dips (70-90°) toward NE. On the foliation plane, mineral lineation is slightly oblique and shows a gently to moderate (30-80°) plunge toward NW or NNE (Fig. 3). Plagiogranite veins lie parallel to the main foliation documented in peridotites and gabbros, whereas basalt dikes cross cut at low angle the main foliation.

At the mesoscale, two main fabrics were documented exclusively in peridotites: proto-tectonites (PF1) (Figs. 3, 4 and 5a), mainly preserved in the eastern portion of the CSZ and tectonites (PF2) (Figs. 3, 4 and 5a, b), in the central and western portions of the CSZ. The tectonitic fabric is evidenced by elongated olivine and pyroxene crystals (0.4 - 1 cm; Figs. 5a, b). Gabbros recorded a strongly partitioned mylonitic fabric (Figs. 3 and 5c, d) that produced a network of ultramylonites and mylonites (GF2; Fig. 4) locally preserving lenses of coarse-grained, poorly deformed gabbro (GF1 in Fig. 4). Both gabbros and peridotites recorded a lower temperature mylonitic event (PF3 and GF4; Fig. 4) that produced a continuous and/or anastomosed mylonitic foliation highlighted by acicular amphibole crystals (Figs. 4 and 5b). This mylonitic foliation trends parallel to the previous fabrics. Several meter thick tremolite-bearing shear zones occur mainly at the boundary between peridotites and gabbros (Figs. 3) producing tremolitites in peridotites and cm-thick green phyllonites in gabbros (Figs. 5e, f). The foliation (N140-150°E) within the localized

ACCEPTED MANUSCRIPT

shear zone envelops centimeter to meter thick- lenses of peridotites and gabbros showing an internal foliation (PF2 and GF2) discordant with the external one (Figs. 5e, f).

5.1.1. Geometric relationships between CSZ and Miocene intrusive rocks

The stack of the Apenninic tectonic units and the Miocene emplacement of the Mt. Capanne pluton were responsible of the actual trend and position of CSZ. Notwithstanding the vertical exposure of the outcrops, the crosscutting relations between the CSZ fabrics/structures and the Miocene intrusive rocks are well exposed in the field.

The porphyry delimiting the western boundary of the CSZ transposed the mylonitic fabrics documented in the peridotite-gabbro sequence (PF2, PF3, GF2; Fig.6a). Close to the porphyry, in fact, the tectonite/mylonite foliation becomes parallel to the sub-magmatic foliation documented in the porphyries whereas few meters away they form and angle of c. 60-70° (Fig.6a). At the western boundary instead, mylonitic foliation in gabbros (GF2) (Fig. 3) and sub-magmatic foliation in porphyry show an apparent parallelism induced by the vertical exposure of the cliff. Moreover, approximately in the central portion of the CSZ, an E-W trending meter-thick undeformed granitic dyke (Fig. 3) crosscuts the mylonitic foliations in sheared peridotites and gabbros (Fig. 6b) and contains decimeter-thick angular enclaves of tectonite peridotite (PF1), high-temperature mylonite peridotites (PF2) and mylonitic gabbro (GF2) (Fig. 6c). These geometrical relationships imply that the intrusion of the Miocene magmatic rocks occurred in an already sheared basement. This timing is also confirmed by the static growth of euhedral gedrite – anthophyllite crystals (50-400 μm), induced by the pluton emplacement, onto all the fabrics documented in the CSZ (see Section 6 for detailed descriptions).

5.2. Serpentinization processes

ACCEPTED MANUSCRIPT

Serpentine minerals (both in the veins and in the groundmass) were documented mainly in the eastern portion of the CSZ (*c.* 5% of rock volume) and close to the m-thick tremolite-bearing shear zones. These veins show a maximum of 3 cm in thickness and 35 cm in length and are partly or completely replaced by magnetite. In the westernmost sector of the CSZ, fibrous serpentine fills mm- to sub-millimeter tabular veins whereas cm-thick veins filled by lizardite and talc developed discordantly to the foliation associated to the tremolite-bearing localized shear zones (PF5) (see Appendix 2 for XRDp results and field photo). The lenticular and tabular veins cross cut the proto-tectonite (PF1) and the tectonite foliation (PF2). The geometrical relationships between lower-temperature foliation (PF4-GF3) and serpentine veins are more complex. The tabular veins seem to postdate the low-temperature foliation (PF4) in the lower strain domains whereas it seems to be interrupted in correspondence of the cm-thick localized strain domains (Fig. 5b).

5.3. LA-ICP-MS U-Pb dating results

In the selected plagiogranite vein (see Appendix for a detailed sample description), zircon commonly occurs as aggregates of euhedral grains aligned parallel to the foliation and mainly associated with biotite. Inclusions and fractures, with or without fragment displacement, are frequent. Zircon grains in CL have oscillatory and sector zoning typical of growth under magmatic conditions and brighter CL domains locally occur crosscutting the zircon grains from the edges to the inner domains (see Appendix 4). These brighter domains probably testify a fluid-assisted recrystallization process.

A total of thirty analyses were collected on twenty-eight zircon grains (see Appendix 4): thirteen analyses were performed using a spot size of 25 μm and seventeen at 10 μm. U-Pb data are mainly discordant and define three main alignments on the Tera-Wasserburg diagram, with lower intercepts at about 201Ma, 173 and 160Ma (Fig. 7a). The observed discordance of the data can be related to crystal-plastic deformation of zircon at amphibolite-facies metamorphic conditions (e.g.

ACCEPTED MANUSCRIPT

Timms et al., 2006; Piazolo et al., 2012). Only eight data resulted concordant at 195 ± 11Ma, 183 ± 12Ma, 178 ± 9Ma, 174 ± 7Ma, 173 ± 6Ma, 172 ± 11Ma, 172 ± 6Ma and 161 ± 6 Ma (2σ error) with a weighted average age of the main cluster at about 174Ma (Fig. 7b). Integrating CL features and U-Pb data, we suggest that zircon grains indicate a main magmatic event at about 174Ma with a later perturbation of the U-Pb system 10 Ma later. The old U-Pb concordant data and the lower intercept age at about 200Ma may be interpreted as due to partial resetting of inherited zircon grains.

6. Microstructures

The summary of the fabrics documented at meso and microscopic scale in gabbros and peridotites of the CSZ is showed in Fig. 4. In addition to the fabric documented at the meso-scale, we recognized at the microscopic scale an olivine + spinel + ilmenite mylonitic fabric in peridotites (PF3 in Fig. 4) and a metasomatic event (phlogopite blastesis) in both peridotites and gabbros (see Section 6.3).

Microstructural analysis was used to refine and confirm mesoscopic observations and to define mineral parageneses associated to the different foliations. Three fabrics were exclusively documented in the peridotites (proto-tectonites, PF1, tectonites, PF2, mylonites, PF3) and two in the gabbros (metagabbros, GF1, and mylonite/ultramylonites, GF2). These fabrics are then overprinted by a metasomatic event that produced the growth of phlogopite. A later mylonitic event that produced Amph - bearing mylonite (PF4 and GF3, in peridotites and gabbros respectively) and the tremolite – bearing, metric localized shear zones (PF5 and GF4) overprint and partly obliterate, all the previous fabrics. Static euhedral amphiboles (50-500 μm) with gedritic composition overprint previous metamorphic associations and are interpreted as evidence of the contact metamorphism related to the Mt. Capanne pluton emplacement. To describe chronologically the different fabrics and metamorphic events, we first present the fabrics documented exclusively in the peridotites and

ACCEPTED MANUSCRIPT

in the gabbros and then we describe the metasomatic blastesis and the Amph -bearing shear fabrics documented in both lithotypes.

6.1. Peridotites

6.1.1. Proto-tectonite (PF1)

Proto-tectonites (PF1 in Fig. 4) consist mainly of olivine (87-88 Fo%), orthopyroxene (87-90 En%), clinopyroxene and Cr-rich spinel (Table 1). Olivine shows heterogeneous grain size distribution with slightly elongated grains parallel or at small angle to the main foliation. It generally shows weak undulose extinction, amoeboid boundaries with embayment structures and sub- and new grains up to 100-250 μm in size (Fig. 8a). These microstructures indicate grain boundary migration recrystallization mechanisms. Occasionally, olivine shows granular texture (Fig. 8a). Pyroxene in contact with olivine crystals generally shows curvilinear and amoeboid grain boundaries, suggesting that mantle pyroxene was partly replaced by a late olivine growth. Within the granoblastic portion of the rocks, spinel occurs as euhedral zoned crystals whereas skeletal spinel is preserved elsewhere.

6.1.2. Tectonites (PF2)

Tectonite peridotites (PF2 in Fig. 4) consist mainly of olivine (81-84 Fo%; Table 1), spinel and Mg-rich ilmenite (Figs. 8b-d). Olivine and spinel generally occur as less than 1 mm thick ribbons that are locally boudinaged and have a maximum aspect ratio of 10:1 (Figs. 8b, c). The thicker ribbons often consist of monocrystalline olivine grains (0.7-1.5 mm) that show weak undulatory extinction, weak shape preferred orientation with long axis parallel to the ribbon boundaries and microfractures oriented orthogonal to the ribbon boundaries. The thinner ribbons are made by either elongated olivine grains (0.8-1 mm) or by granoblastic aggregates of olivine and spinel with size up to 50 μm, that locally show 120° triple junctions and no evidence of

ACCEPTED MANUSCRIPT

intracrystalline deformation (Fig. 8d). Spinel occurs in two different textural positions: within the olivine ribbon as equigranular grains (20-50 μm) with straight grain boundaries (Fig. 8d) and homogeneous composition, and as elongated grains (100-200 μm) oriented parallel to the olivine-spinel ribbons (Figs. 8c, d). Mg-rich ilmenite grains are partly fractured and are up to 1mm (Fig. 8c). Very small (50-80 μm) relicts of clinopyroxe have been rarely documented. The tectonite fabric is overprinted by two later mylonitic events (i.e. PF3 and PF4 in Figs. 3 and 4; see sections below).

6.1.3. High temperature mylonites (PF3)

The transition between tectonites and mylonites is fairly sharp and it is marked by an abrupt grain size reduction. The mylonitic foliation (PF3 in Fig. 4) is made of very fine-grained olivine (20-50 μm; 88-90 Fo%; Table 1) and (rare) orthopyroxene (~20 μm) neoblasts, without evidence of intracrystalline deformation, associated to elongated spinel and ilmenite grains (Fig. 10). The mylonitic foliation wraps large (0.6-1.2 mm) ortho- and clinopyroxene grains (interpreted as relicts of proto-tectonites; Fig. 9) and locally asymmetric polycrystalline olivine ribbons (interpreted as relicts of tectonites; Figs. 9a, b). Occasionally the pyroxene porphyroclasts are kinked and are partly replaced by amphibole (Fig. 9a), olivine lamellae and olivine embayments (Figs. 8b-d). The olivine ribbons themselves wrap the clinopyroxene grains (Figs. 9a, b). In the thicker ribbons (>500μm), olivine crystals show heterogeneous grain size (up to 250 μm), weak shape preferred orientation, oblique to the external mylonitic foliation, and occasionally granular texture with 120° triple junctions, testifying that local grain growth and annealing processes were active (Fig. 9a). In some ribbons, olivine shows homogeneous grain size distribution (150-200μm) with aspect ratio (long axis/short axis) of 3:1, undulatory extinction and strong shape preferred orientation with long axis parallel or oblique (<35°) to the mylonitic foliation (Fig. 9b). Euhedral olivine neoblasts (~ 20 μm in size) and (rare) anorthite (~ 30 μm) have been instead documented in the pressure shadows (Fig. 9c) and inside fractures oriented orthogonal to the high temperature mylonitic foliation, both in Mg-rich ilmenite and clinopyroxene porphyroclasts.

ACCEPTED MANUSCRIPT

6.2. Metagabbros

6.2.1. Magmatic fabrics (GF1)

Magmatic fabrics (GF1 in Fig. 4) are preserved as centimeter thick pods within the mylonites and ultramylonites fabric (Figs. 5c, d). GF1 fabric consists of an association of medium to coarse-grained plagioclase (50-48An%) and pyroxene euhedral crystals (40-60En%; Table 1), ranging in size from 0.5 to 2 mm (Fig. 10a) showing evidence of weak dynamic recrystallization.

6.2.2. High temperature mylonites (GF2)

High temperature mylonite (and ultramylonite) fabrics (GF2 in Fig. 4) form an anastomosed network of high-strain domains that envelop lenses of less deformed gabbros (Figs. 3 and 10). Mylonite fabric (Fig. 10b) is marked by flattened aggregates of iso-oriented pyroxene (700 - 300 μm) and plagioclase (1.5 mm - 300 μm) crystals defining the main foliation. Plagioclase porphyroclasts show undulatory extinction, deformation twinning and very-small sub- and new-grains indicating intracrystalline deformation and dynamic recrystallization under temperatures of 450-600°C (Passchier and Trouw, 2006). Pyroxenes locally show kink, undulatory extinction and very thin rims of fine-grained new-grains (10-20 μm) indicating the action of intracrystalline deformation and sub-grain recrystallization.

The ultramylonite fabric (Figs. 10c, d) is marked by fine-grained layers (~80-200 μm –thick) made of plagioclase (50-63An%) and pyroxene + plagioclase (±titanite), characterized by homogeneous grain size (10-40 μm), straight boundaries and elongated parallel to the mylonitic foliation (Fig. 10d). Pyroxene relicts, mainly preserved within the thicker plagioclase ribbons, are strongly fractured and boudinaged, with amoeboid boundaries resulting from both reactions (the biggest grains show rims (? embayments) of ~10 μm plagioclase grains) and sub-grain boundary

ACCEPTED MANUSCRIPT

recrystallization (Figs. 10c, d). The transition between mylonite and ultramylonite is gradual and marked by a change in grain size and in the degree of shape preferred orientation.

6.3. Phlogopite metasomatic event

Tectonite peridotites (PF2), mylonite peridotites (PF3) and mylonite/ultramylonite gabbros (GF2) are affected by metasomatic blastesis of phlogopite (Figs. 4 and 10a, b). In GF2, phlogopite crystals (20-100 μm) grew in 30 μm – 1 mm thick layers along the mylonitic/ultramylonitic foliation (Fig. 11c). Rarely, phlogopite is found in veins cross-cutting the main foliation (Fig. 10d). Locally, it wraps elongated plagioclase and pyroxene crystals. In strained plagioclase affected by bookshelf structures, phlogopite grew along the crystal fractures (in association with very small plagioclase new grains) (Fig. 11d). In ultramylonites, phlogopite grew in pressure shadows (associated to ilmenite) and in weak asymmetric tails around rigid plagioclase + pyroxene aggregates (Fig. 10c). However, even though most of the phlogopite crystals grew parallel to the earlier mylonitic foliation (i.e. GF2), several small crystals (200-300 μm) are oriented orthogonally to it (Fig. 11d).

6.4. Lower-temperature mylonites (PF4 and GF3)

Lower-temperature mylonites (PF4 and GF3 in Fig. 4) consist of strongly aligned fibrous and/or acicular Ca-rich amphibole grains showing heterogeneous grain size (50- 500 μm) and composition ranging from Mg-hornblende to tremolite-actinolite (Fig. 12a; Table 1). These mylonites, developed heterogeneously along the CSZ (Fig. 3), are poorly developed in metagabbros and proto-tectonites peridotites whereas they are widespread in tectonite (PF2) and mylonite peridotites (PF3) (Figs. 8a-d, 9a, b, d, 10b and 11a, b). In the spaced domains in tectonite and mylonite peridotites, the foliation is marked by discontinuous and 50 μm – 1 mm thick amphibole-

ACCEPTED MANUSCRIPT

rich layers that envelop sub-rounded to elongate olivine and orthopyroxene (1 – 0.5 mm in size) (Figs. 8b-d and 8a, b, d). In mylonite gabbros, acicular amphibole crystals bound elongated plagioclase and clinopyroxene porphyroclasts (Figs. 10d and 11d) and fill the necks of boudinated plagioclase (Fig. 12b) testifying their growth contemporaneous to microfracturing. The Ca-amphibole crystals overprint phlogopite crystals, grown during the metasomatic event, and plagioclase (Fig. 11a).

6.5. Tremolite-bearing shear zones (PF5 and GF4)

The m-thick localized shear zones developed at the boundary between gabbros and peridotites (Figs. 3 and 5) are characterized by a continuous mylonitic foliation and by 0.7 to 1.2 mm-spaced C -type shear bands marked by fine-grained (60 – 100 μm) tremolite crystals (Fig. 12c) characterized by well-developed shape and crystal preferred orientation.

7. Olivine and amphibole quantitative LPO

7.1. Quantitative Texture Analysis (QTA) data description

Fig. 13 shows the Lattice Preferred Orientations (LPO) of amphibole and olivine in three peridotite samples representative of PF1 (sample COT14), PF2 (sample COT18) and PF3 (sample COT16) (see Fig. 3 for samples location and Appendix Fig. 3). In Fig. 13 LPO are displayed as pole figures where the three main fabric axes are represented with the XZ plane being the figure plane and the XY plane the orthogonal to the pole figure, with X axis being the horizontal direction. Moreover, the crystallographic axes and angles are shown to better visualize the pole figure relations. Pole figures represent the normal directions to specific planes of Bragg and they may or may not coincide with crystallographic directions, as explicitly declared in Fig. 13. For the

ACCEPTED MANUSCRIPT

orthorhombic olivine all the normal poles correspond to regular crystallographic axes whereas for the monoclinic amphibole this is true only for the normal (pole) to (010) or {*0k0*} planes.

7.1.1. Amphibole

The three samples are characterized by similar LPOs, where the pole to (100) is almost parallel to the Z-axis, with this parallelism being more evident in the COT18 sample. Pole to (010) (i.e. [010] axis), is less clustered, with a slightly defined maximum close to the X axis and a girdle close to the XZ plane in the COT14 and COT16 samples, while for COT18 the girdle is normal to XZ plane and at ≈10 degrees to X. The normal to (001) displays a well-defined cluster close to the Y axis in COT16; this cluster is broader in COT14 where a girdle develops almost parallel to the XY plane. COT18 displays a similar girdle parallel to the XY plane, with a <10 degrees to X, but the cluster is absent. The described textures have been already described in amphibolites and amphibole-bearing schist worldwide (Siegesmund et al., 1994; Imon et al., 2004; Barberini et al., 2007; Zhang et al., 2013; Zucali et al., 2014; Getsigner and Hirth, 2014) and are typically related to amphibolite to granulite facies conditions (T = 650 - 800°C) at relatively low pressures (0.4 - 0.8 GPa).

6.1.2. Olivine

Olivine LPO in PF1 and PF2 fabrics (COT14 and COT18) is characterized by [100] axes that plot at ≈10 to 30 degrees to the X direction in the XZ plane and at ≈10 degrees in the XY plane, producing a cluster at low angle to the lineation X. Correspondingly, [010] axes define a girdle close to the YZ plane, with a weak maximum at ≈70 degrees to the X direction in the XZ plane and ≈80 degrees in the YZ plane (Fig. 13). Conversely, PF3 fabric (COT16) displays a disperse distribution of the main crystallographic axes, though [001] defines a cluster close to the Y axis, with a dispersion along the XY plane. PF1 and PF2 LPO distributions are typical for high temperature (T >800°C) olivine deformation, as described for olivine under variable stresses and

ACCEPTED MANUSCRIPT

water contents (Jung et al., 2006; Karato et al., 2008; Mainprice 2007; Warren et al., 2008). The disperse olivine LPO developed in PF3 mylonite and associated with amphibole LPO may be ascribed to a general decrease in temperature, below 800°C.

8. Discussions

8.1. The Cotoncello Shear Zone: reconstructing the deformation along a fossil oceanic detachment fault

Considering that (1) the ophiolite sequences cropping out in western Elba Island are classically interpreted as representative of a typical oceanward section of Western Tethys oceanic lithosphere (i.e. the Internal Ligurian Units), (2) we documented the presence of HT ductile fabrics both in gabbro and peridotites and (3) the almost complete lack of a widespread and diffuse water-rock interaction (as instead documented on the seafloor exposed at the surface in modern OCC), we suggest that the CSZ represents the deep root of a fossil oceanic detachment fault developed in a slow spreading oceanic domain. In analogy with the Kane OCC on the Mid-Atlantic ridge (Hansen et al., 2015), the CSZ preserves evidences of a dominant high-temperature viscous deformation developed under low-pressure granulite to upper amphibolite facies conditions (e.g. fabrics PF1-PF3 and GF1-GF2; Fig. 4) lately overprinted by brittle-ductile localized shear zones.

After an early event during which peridotites were affected by recrystallization of olivine (in elongated ribbon) and spinel + ilmenite ± orthopyroxene (Fig. 14a, t1), gabbros and peridotite shared the same history. After the emplacement of gabbros (slightly before *c.* 170Ma) the entire oceanic lithosphere section was affected by a mylonite event (PF3-GF2; Fig. 14b, t2) in upper amphibolite facies conditions (Fig. 4). A high-temperature phlogopite metasomatic event related to the gabbro emplacement was documented in both lithotypes. Although, in modern OCCs the occurrence of phlogopite is rarely documented, an example has been reported from an OCC located

ACCEPTED MANUSCRIPT

near the Rodriguez Triple Junction in the Indian Ocean (Soda et al., 2010). The final mylonitic events in the CSZ (PF4-GF3; Fig. 14b, t3) are associated to the widespread growth of Mg-hornblende along a penetrative mylonitic foliation and to the late development of the tremolite-bearing shear zones (PF5-GF4; Fig. 14c, t4) localized manly at the gabbro-peridotite boundaries (Fig. 3). These final deformations took place from lower amphibolite to upper greenschist facies conditions (Fig. 4).

Microstructures and syn-kinematic mineral assemblages indicate that the different mylonitic fabrics are characterized by progressively colder temperature (from granulite to upper greenschist facies). The parallelism existing between HT ductile fabrics (T: 800-600°C) at meso and microscale (PF1-PF4 and GF1-GF3) is consistent with a continuous deformation processes. In particular, a relevant feature is the development of lower temperature foliation (i.e. highlighted by the growth of amphibole PF4 and GF3) in sharp complete structural continuity and parallelism with previous granulite facies foliations marked by preferred growth of olivine and pyroxene (PF1-PF3 and GF1-GF2). Similar features, observed at micro-to mesoscale also in other analogue OCCs (Vauchez et al., 2012; Nicholas et al., 2017), are therefore diagnostic of oceanic detachment faults. Slightly discordant relationships were observed in the localized brittle-fabric shear zones (i.e. PF5 and GF4) where all previous ductile fabrics are crosscut by tremolite-bearing foliation (Figs. 5e, f).

Microstructures indicate that the first event of shearing (PF2) occurred below the plastic-brittle transition at temperature >800°C (as suggested by LPO analyses results; granulite facies). The overprinting of brittle microstructures (e.g. bookshelf in plagioclase; Fig. 11c) on ductile fabrics in both gabbros and peridotite mylonites (PF3 - GF2), indicate that the emplacement of gabbros may have occurred immediately below, or in correspondence to, the brittle-plastic transition (BPT) at temperatures of c. 800°C (Fig. 14, t2 and Fig. 15). In analogy with modern OCCs (Andreani et al., 2007; Hansen et al., 2013), the almost complete absence of serpentines supports the fact that fabrics PF3-GF2 occurred in correspondence, or below, the seismic Moho, characterized by seismic P-waves velocities of c. 8km/sec (e.g. Andreani et al., 2007), at the depth

ACCEPTED MANUSCRIPT

of c. 6-10 km (Fig. 15; e.g. deMartin et al., 2007; McLeod et al., 2009; Hansen et al., 2013). These values are also inferred by works on analogue on land OCCs (e.g. Manatschal et al., 2011) and are coherent with petrographic studies conducted on the gabbroic rocks from Northern Apennine (Piccardo, 1994; Tribuzio et al., 1995).

In our reconstruction, the gabbroic bodies, emplaced within a high-temperature viscous shear zone, probably rooted below the BPT (<6-10km), enhanced the strain softening and the localization at depth of the oceanic detachment fault (ODF) that bounds the OCC. In analogy with the modern OCCs (Tucholke et al., 1998; Dick et al., 2000; deMartin et al., 2007; Hansen et al., 2013), the detachment fault may also root below (or near) the melt rich zone or the magma chamber. The high-temperature shear zones affecting peridotites and gabbros (PF3-GF2) may have acted as conduits for magma-derived fluids that, immediately above the BPT, produced the widespread blastesis of amphibole at temperature between 650 and 800°C (PF4-GF3) (Fig. 14, t3 and Fig. 15). At this depth, seawater-dominant derived fluids and the alteration front may promote efficient deformation localization along the ODF. At shallower crustal level (i.e. close to the sea floor), brittle-ductile shear zones and extensional faults (at the seafloor) may accommodate the flexural rotation of the OCC that is responsible of the exposure of the large portion of lower crust/mantle peridotites and of its dome shape. We suggest that the tremolite-bearing shear zones were developed during this strain accommodation and that the roll-over of the ODF was responsible of the slight discordant relations between these shear zone and the previously ductile fabrics (Fig. 14, t4). The widespread blastesis of tremolite indicates that during this phase temperature was below 500°C. Seawater percolation becomes important and serpentine minerals (and talc) grew within or close the Tr-bearing shear zones as testified by the development of lizardite + talc veins documented in the western sector of the CSZ. In conclusion, the deformation fabrics documented in the CSZ indicate a progressive shearing along a linear rock path during a delamination processes under retrogressive conditions (Vauchez et al., 2012), that involve cooling, changes in deformation conditions and strain localization along a lithospheric shear zone.

ACCEPTED MANUSCRIPT

No evidence of brittle deformation (i.e. cataclasites), pervasive serpentinization related to upper crustal level conditions and exposure at the sea floor levels are recorded in the CSZ. In addition, in the south-central Elba Island (Portoazzurro locality; Fig. 1) the boundary between upper mantle/lower crust and post-extensional sedimentary covers (i.e. pelagic limestones) is marked by serpentinites, dm-thick ophicalcites and ultramafic sedimentary breccias (Barnes et al., 2006). Lithotypes and rock associations similar to those documented in the Portoazzurro area were recently described in the alpine ophiolite units exposed in western Alps and Corsica Island where they are interpreted as produced by extensional tectonics and rock-fluid interactions at the exposed footwall of an oceanic detachment fault (Manatschal et al., 2011; Balestro et al., 2015; Festa et al., 2015; Lagabrielle et al., 2015). In conclusion, the presence of ductile fabrics and the lack of ophicalcites, serpentinites and/or talc-chlorite schists above the upper mantle/lower crust denudated section indicates that the CSZ can be interpreted as an analogous of the deep root of a present-day oceanic detachment fault.

8.2. Timing of gabbro emplacement and ODF activity

Assuming that the magmatic ages obtained in gabbroic rocks from ophiolite units constrain the formation of new oceanic lower crust, it is logic to use these ages to broadly estimate the age of extensional tectonics leading to continental breakup and oceanic spreading. In the last decades the magmatic ages of gabbroic rocks intruded in the Tethyan ophiolite sequences now exposed in the Western Alps and Northern Apennines were intensively investigated (see the reviews of Balestro et al., 2015 and Tribuzio et al., 2016). Nevertheless, the reconstruction of the paleogeography of western Tethys Ocean identifying the sectors of earlier spreading is very difficult and should be done with great caution. The paleogeographic restoration of the oceanic basin, in fact, is strongly biased by the pre-orogenic and orogenic tectonics that dismembered the pristine oceanic

ACCEPTED MANUSCRIPT

architecture. In addition, the alpine metamorphism may have caused perturbations in the U/Pb system. Consequently, individuating a possible trend for magmatic propagation is difficult.

The main zircon U/Pb cluster ages obtained in the gabbros from the Western Alps ophiolite units range from ~166 to ~155Ma (Lombardo et al., 2002; Rubatto and Hermann, 2003), even if the younger ages should be revisited due to the Alpine metamorphism that could led to Pb loss (Tribuzio et al., 2016). The main cluster of ages from the accretion of the lower crust in the Northern Apennines range from 163-160 Ma and 173-161 Ma for the oceanward (i.e. Internal Ligurian Units) and continentalward (i.e. External Ligurian Units) portions, respectively (see review of Tribuzio et al., 2016). According to Tribuzio et al., (2016) the spreading started at c. 161 Ma.

Even if some of the U-Pb ages collected in this study (c. 174Ma) are in agreement with the oldest ages of oceanic Tethyan lithosphere (Internal Ligurian Unit) in Northern Apennines, more geochronological investigations are needed in order to shed light on the complex tectono-magmatic history of these intrusive rocks.

Our data are also coherent with the ages of radiolarian cherts cropping out c. 20 km east of the study area and dated by Chiari et al., (2000) at c. 169-147.7 Ma (*pers. comm.*). The age of these post-extension sediments may so corroborate that the activity of the ODF described in this study is probably older that 169Ma.

8.3. Hydrous phases in the CSZ

Although the sheared rocks of the CSZ were affected by a widespread growth of hydrous phases (e.g. phlogopite and Mg-hornblende/tremolite), they show a very low content of serpentine. This feature strongly contrasts with the rest of ophiolites exposed in the Elba Island (and Northern Apennines) in which serpentine reaches 60-85% of the rocks volume, and an amphibole-bearing foliation is absent. The absence of serpentine and the simultaneous development of HT ductile

ACCEPTED MANUSCRIPT

fabrics seem to support the idea that the studied mantle/crustal section was not exposed at the see floor but instead deformed at depth.

Phlogopite is the older OH-bearing mineral documented in the CSZ. Its blastesis relationships and microstructures indicate the presence of K-enriched fluids during the late stages of PF3/GF2 and absolutely before the development of PF4/GF3. It can be either (1) related to the emplacement of the gabbros (Soda et al. 2010) or (2) a consequence of mobilized seawater fluids (Cortesogno et al., 1994). Considering the lack of serpentine minerals, we suggest that the temperature during the metasomatic event was higher than that of the serpentine stability field (T > 500°C) and that the K-metasomatism occurred with negligible seawater component.

The second OH-bearing phase observed in the CSZ is Mg-hornblende. It may be produced by fractional crystallization process following the formation of gabbroic cumulates deeply in the crust with a limited contribution of seawater (Flagler and Spray, 1991; Bach et al., 2004; Koepke et al., 2004, 2007). In addition, LPO analyses indicate that amphibole grew at temperatures lower than 800°C. The poorly developed network of serpentine veins, now partly or completely replaced by magnetite, may corroborate this hypothesis. In fact, serpentine can be partially or completely replaced by magnetite, with consequent production of Si-enriched fluids, by reaction (Frost and Beard, 2007):

serpentine = magnetite + silica + H_2O + H_2 (1)

This evolution is consistent to what suggested by Mellini et al., (2005) that described, in the eastern Elba Island, magnetite replacing poorly crystallized lizardite + chrysotile-bearing veins (grown during the early stage of oceanic metamorphism at temperature above 350-400°C). The thin tabular veins of fibrous serpentine documented in the western outcrops of the CSZ may be produced during minor, very late, episodes of deformation. In agreement with the reconstruction of Cortesogno et al. (1994), we suggest that close to the exposure at the seafloor, hydrothermal activity localized within the tremolite-bearing meter-thick shear zones, may have induced Si-metasomatism

ACCEPTED MANUSCRIPT

and consequent precipitation of talc in the cm-thick veins (see Appendix 2) by reaction (Bach et al., 2004):

serpentine + silica = talc + H_2O (2)

Si may derive by reaction (1) and be transported at shallow structural levels along the localized shear zones (PF4 and GF3). Tribuzio et al. (2014), on the other hand, suggest that since the Ligurian Tethys is classically interpreted as a slow-/ultraslow seafloor spreading basin, Si probably derived from high-temperature water-rocks reactions (Bach et al., 2004; Ray et al., 2009) triggering partial melting of gabbros under greenschist facies conditions.

8.4. Comparison with modern OCC and present-day slow spreading ridge

OCCs are dome-shaped structures bounded by normal faults (i.e. ODF) trending parallel to the spreading axes and characterized by km size apparent offsets. The fault motion and its later flexural rotation occur at the same time of denudation and uplift of the lower crust/upper mantle sections when the volume of magma production is insufficient to accommodate extensional rates along slow- ultraslow spreading ridges (i.e. Mid-Atlantis Ridge and Southwest Indian Ridge). The rock suites derived from different lithospheric levels and exposed at the fault surface are deeply altered as a consequence of pervasive interaction between faulting, fault rocks and fluids, producing serpentinites and ultimately talc-tremolite-chlorite schists (e.g. Tucholke et al., 1998; Boschi et al., 2006; Escartín et al., 2008; MacLeod et al., 2009).

The partitioning, the strength and the kinematic evolution of shear deformation along the ODF have been investigated by several authors in the last decades documenting a dominant brittle deformation with pervasive development of secondary hydrous phases (e.g. MacLeod et al., 2002; Escartín et al., 2003; Harigane et al., 2008). On the other hand, very few authors have documented the presence of diffuse high-temperature viscous deformation (e.g. Dick et al., 2000; Mehl and Hirth 2008; Miranda and Jones, 2010; Hanson et al., 2013). In particular along the Mid-Atlantis

ACCEPTED MANUSCRIPT

Ridge, 100 to 400 m thick high-temperature ductile shear zones were documented below a thinner volume of rocks affected by brittle deformation (Karson et al., 2006; Mehl and Hirth 2008; Miranda and John, 2010; Hansen et al., 2013). For example, in the Kane OCC, Hansen et al. (2013) described crystal-plastic deformation at T > 700°C and suggested that the ODF rooted below or into the brittle-plastic transition.

In the Jurassic ophiolites exposed in Western Elba, only scarce low-temperature hydrothermal alterations are described (e.g. the Tr-bearing shear zone in the CSZ) and neither ophicalcites nor reworked tectonic breccias have been documented between the sheared peridotites and gabbros and the marine deposits. Our observations indicate that small bodies of gabbros were intruded below or in correspondence of the brittle-plastic transition at T ≈ 800 °C and depth of 6-10 km within an early ductile high-temperature shear zone rooted at depth in the upper mantle peridotites (Figs. 14 and 15). This reconstruction is broadly in agreement with those proposed by Hansen et al., (2013) and Dick et al., (2010) at the Kane OCC (MAR) and at the Southern Indian Ridge, respectively, whereas it contrasts with other studies in which ductile fabrics were not related with the ODF activity (e.g. Escartín et al., 2003; Manatschal et al., 2011).

Along different sections across the Mid Atlantic Ridge, earthquake hypocenters reach maximum depths of *c.* 7-8 km (e.g. Toomey et al., 1988; deMartin et al., 2007; Mcleod et al., 2009). P-waves velocity models used to define these hypocenters show that at this depth Vp is *c.* 8km/sec (e.g. Canales et al., 2000; deMartin et al., 2007). Vp models used in natural OCCs and studies linking serpentine content and seismic waves (e.g. Canales et al., 2000; Escartin et al., 2001; Andreani et al., 2007) indicate that at *c.* 8km/sec, which for definition marks the seismic Moho, serpentine is absent (Fig. 15). As in the CSZ, serpentine was not present during the pervasive shearing (i.e. PF1, PF2 and PF3 in peridotites and GF1 and GF2 in gabbros), we suggest that the CSZ activity started deep in the lithosphere in correspondence or slightly below the seismic Moho (i.e. the brittle-ductile transition; Fig. 15).

ACCEPTED MANUSCRIPT

Rock associations analogous to what documented at the exposed surface of modern (e.g. Boschi et al., 2006) and ancient (Balestro et al., 2015; Festa et al., 2015; Lagabrielle et al., 2015) OCCs were documented c. 15 km east/southeast respect to the CSZ in the Portoazzurro area (Fig. 1) where c. 30 cm-thick ophicalcites are covered by 40-50 cm of debris flow deposits, interlaid between sheared serpentinites and radiolarian cherts/pelagic deposits (Barnes et al., 2006). It is worth to note, however, that the collisional and post-collisional tectonics affecting the Elba Island have strongly dismembered the original architecture of the Jurassic oceanic seafloor.

10. Conclusions

We report the first description of a hundred-meter thick mylonite zone (Cotoncello Shear Zone) affecting a lower crust/mantle section exposed in the western Elba Island (Italy). The sequence, typical of a slow-/ultraslow spreading ridge setting, was not affected by the orogenic deformation and metamorphism related to the Apennines orogeny and was only tilted by the Mt. Capanne pluton emplacement. In the studied section, the contact metamorphism is limited to the static growth of gedrite crystals.

Field and microstructural data associated to lattice preferred orientation measurements and U-Pb zircon geochronology led us to constrain how tectonics, magmatism and hydrothermal processes enhanced the strain localization during the OCCs evolution. The U-Pb zircon ages determined in the plagiogranite dyke suggest that the ophiolites exposed in the western Elba island were produced during an incipient phase of spreading and that the reopening of U-Pb system at ~160Ma may be due to a later magmatic episode. Between these two episodes of magmatism, extension was mainly accommodated by tectonics with the localization of deformation along an oceanic detachment fault (ODF) (i.e. OCC activity). We suggest that during this amagmatic phase, the ODF rooted below the plastic-brittle transition. Our results indicate that the spatial and temporal localization and activity of the ODF were controlled by different parameters (i.e. gabbroic intrusions, magmatic fluids,

ACCEPTED MANUSCRIPT

temperature, seawater content) and that the mechanism and rheology of the detachment changed during the exhumation path. In analogy to what recently documented in the Kane oceanic core complex on the Mid-Atlantic Ridge (Hansen et al., 2013), we conclude that the CSZ may therefore represent an excellent laboratory to investigate on land the deep root of an OCC and the relationships between magmatism and deformation developed at different structural levels during the activity of the ODF.

Acknowledgements

We thank A. Festa and an anonymous reviewer for the constructive criticisms that helped to improve the manuscript and M. Scambelluri for the careful editorial work. The authors thank M. Pompilio (INGV) for his support during the SEM investigations, C. Gini for the help with XRPD interpretation and M. Chiari (IGG-CNR, Firenze) for clarifications about the age of radiolarian cherts in the Elba island. CF thanks S. Rocchi for introducing her to the sheared ophiolite sequences in western Elba and L. Pandolfi, M. Marroni and S. Rocchi for constructive discussions. MZ thanks Bachir Ouladdiaf for technical and scientific support at Institut Laue-Langevin for neutron texture analysis. This work was supported by PRA 2016 project (S. Rocchi; Università di Pisa).

References

Andreani, M., Mevel, C., Boullier, A.-M., Escartín, J., 2007. Dynamic control on serpentine crystallization in veins: Constraints on hydration processes in oceanic peridotites. Geochemistry, Geophysics, Geosystems 8, Q02012, doi:10.1029/2006GC001373.

Bach, W., Garrido, C.J. Paulick, H., Harvey, J., Rosner M., 2004. Seawater-peridotite interactions: First insights from ODP Leg 209, MAR 15°N. Geochemistry, Geophysics, Geosystems 5, Q09F26.

Balestro G., Festa, A., Dilek, Y., Tartarotti, P., 2015. Pre-Alpine extensional tectonics of a

ACCEPTED MANUSCRIPT

peridotite localized oceanic core complex in the Late Jurassic, high-pressure Monviso ophiolite (Western Alps). Episodes 38, 266-282.

Barberi F., Innocenti F., 1965. Le rocce cornubianitico-calcaree dell'anello termometamorfico del Monte Capanne (Isola d'Elba). Atti Società Toscana di Scienze Naurali, Memorie, Serie A 72, 306-398.

Barberi F., Innocenti F., 1966. I fenomeni di metamorfismo termico nelle rocce peridotitico-serpentinose dell'aureola del Monte Capanne (Isola d'Elba). Periodico di Mineralogia 25, 735-768.

Barboni, M., Annen, C., Schoene, B., 2015. Evaluating the construction and evolution of upper crustal magma reservoirs with coupled U/Pb zircon geochronology and thermal modeling: A case study from the Mt. Capanne pluton (Elba, Italy). Earth and Planetary Science Letters 432, 436–448

Barberini, V., Burlini, L., Zappone, A., 2007. Elastic properties, fabric and seismic anisotropy of amphibolites and their contribution to the lower crust reflectivity. Tectonophysics 445, 227–244.

Barnes, J.D., Selvestone, J., Sharp, Z.D., 2006. Chlorine isotope chemistry of serpentinites from Elba, Italy, as an indicator of fluid source and subsequent tectonic history. Geochemistry, Geophysics, Geosystems 7, Q08015.

Bortolotti V., Cellai D., Martin S., Principi G., Tartarotti P., Vaggelli G., 1994. Ultramafic rocks from the eastern Elba island ophiolites (Tyrrhenian Sea, Italy). Memorie Società Geologica Italiana 48, 195-202.

Boschi, C., Fr€uh-Green, G.L., Delacour, A., Karson, J.A., Kelley, D.S., 2006. Mass transfer and fluid flow during detachment faulting and development of an oceanic core complex, Atlantis Massif (MAR 30°N). Geochemistry, Geophysics, Geosystems 7, Q01004.

Bouillin, J.P., 1983. Exemples de deformation locale liées à la mis en place de granitoides alpins dans des conditions distensives: l'ile d'Elbe (Italie) et le Cap Bougaron (Algérie). Revue de

ACCEPTED MANUSCRIPT

geologie dynamique et de geographie physique 24, 101–116.

Canales, J. P., Collins, J. A., Escartín, J., and Detrick, R. S., 2000. Seismic structure across the rift valley of the Mid-Atlantic ridge at 23°20′N (MARK area): Implications for crustal accretion processes at slow-spreading ridges. Journal of Geophysics Research, 105, 28411–28425.

Cann, J.R., Blackman, D.K., Smith, D., McAllister, E., Janssen, B., Mello, S., Avgerinos, E., Pascoe, A.R., Escartin, J., 1997. Corrugated slip surfaces formed at ridge-transform intersections on the Mid-Atlantic Ridge. Nature 385, 329–332.

Chiari, M., Marcucci, M., Principi, G., 2000. The age of the radiolarian cherts associated with the ophiolites in the Apennines (Italy) and Corsica (France): a revision. Ofioliti 25, 141-146.

Cortesogno, L., Gaggero, L., Molli, G., 1994. Ocean floor tectono-metamorphic evolution in the Piedmont-Ligurian Jurassic basin: a review. Memorie Società Geologica Italaliana 48, 151-163.

deMartin, B. J., Sohn, R. A., Canales, J. P., and Humphris S., 2007. Kinematics and geometry of active detachment faulting beneath the Trans-Atlantic Geotraverse (TAG) hydrothermal field on the Mid-Atlantic Ridge. Geology, 35, 711–714.

Dini, A., Innocenti, F., Rocchi, S., Tonarini, S., Westerman, D.S., 2002. The magmatic evolution of the laccolith- pluton-dyke complex of Elba Island, Italy: Geological Magazine, 139, 257–279.

Escartín, J., Hirth, G., and Evans B, 2001. Strength of slightly serpentinized peridotites: Implications of the tectonics of oceanic lithosphere. Geology, 29, 1023–1026.

Escartín, J., Smith, D.K., Cann, J., Schouten, H., Langmuir, C.H., Escrig, S., 2008. Central role of detachment faults in accretion of slow-spreading oceanic lithosphere. Nature 455, 790–794.

Festa, A., Balestro, G., Dilek, Y., Tartarotti, P., 2015. A Jurassic oceanic core complex in the high-pressure Monviso ophiolite (western Alps, NW Italy). Lithosphere, 7, 646-652.

Flagler P.A., Spray J.G., 1991. Generation of plagiogranite by amphibolite anatexis in oceanic shear zones. Geology 19, 70–73.

Frost B.R., Beard J.S., 2007. On silica activity and serpentinization. Journal of Petrology 48,1351–1368.

ACCEPTED MANUSCRIPT

Getsinger, A.J., Hirth, G., 2014. Amphibole fabric formation during diffusion creep and the rheology of shear zones. Geology 42, 535–538.

Hansen L.N., Cheadle, M.J., John, B.E., Swapp, S.M., Dick, H.J.B., Tucholke, B.E., Tivey, M.A., 2013. Mylonitic deformation at the Kane oceanic core complex: Implications for the rheological behavior of oceanic detachment faults. Geochemistry, Geophysics, Geosystems 14, 3085–3108.

Harigane, Y., Michibayashi, K., Ohara, Y., 2008. Shearing within lower crust during progressive retrogression: Structural analysis of gabbroic rocks from the Godzilla Mullion, an oceanic core complex in the Parece Vela backarc basin, Philippine Sea. Tectonophysics 457, 183–196.

Imon, R., Okudaira, T., Kanagawa, K., 2004. Development of shape- and lattice-preferred orientations of amphibole grains during initial cataclastic deformation and subsequent deformation by dissolution-precipitation creep in amphibolites from the Ryoke metamorphic belt, SW Japan. Journal of Structural Geology 26, 793–805.

Jung, H., Katayama, I., Jiang, Z., Hiraga, T., Karato, S., 2006. Effect of water and stress on the lattice-preferred orientation of olivine. Tectonophysics 421 1–22.

Karato, S., Jung, H., Katayama, I., Skemer, P., 2008. Geodynamic significance of seismic anisotropy of the upper mantle: new insights from laboratory studies. Annual Review of Earth and Planetary Sciences 36, 59.

Karson, J., Fr€uh-Green, G.L.,. Kelley, D.S,. Williams, E.A, Yoerger, D.R., Jakuba, M., 2006. Detachment shear zone of the Atlantis Massif core complex, Mid-Atlantic Ridge, 30°N, Geochemistry, Geophysics, Geosystems 7, Q06016.

Keller, J.V.A., Pialli, G., 1990. Tectonics of the Island of Elba: a reappraisal. Bollettino della Società Geologica Italiana 109, 413-425.

Koepke, J., Feig, S.T., Snow, J., Freise, M., 2004. Petrogenesis of oceanic plagiogranites by partial melting of gabbros: an experimental study. Contribution Mineralogy and Petrology 146, 414–432.

ACCEPTED MANUSCRIPT

Koepke J., Berndt J., Feig, S.T., Holtz, F., 2007. The formation of SiO2-rich melts within the deep oceanic crust by hydrous partial melting of gabbros. Contribution Mineralogy and Petrology 153, 67–84.

Lagabrielle, Y., Vitale Brovarone, A., Ildefonse, B., 2015. Fossil oceanic core complexes recognized in the blueschist metaophiolites of Western Alps and Corsica. Earth Science Reviews 141, 1–26.

Lombardo, B., Rubatto, D., Castelli, D., 2002. Ion microprobe U-Pb dating of zircon from a Monviso metaplagiogranite: Implications for the evolution of the Piedmont-Liguria Tethys in the Western Alps. Ofioliti, 27, 109-117.

MacLeod, C. J., et al., 2002. Direct geological evidence for oceanic detachment faulting: The Mid-Atlantic Ridge, 15°45'N. Geology 30, 879–882.

MacLeod, C.J., Searle, R.C., Murton, B.J., Casey, J.F., Mallows, C., Unsworth, S.C., Achenbach, K.L., Harris, M., 2009. Life cycle of oceanic core complexes. Earth and Planetary Science Letters 287, 333–344.

Mainprice, D., 2007. Author ' s personal copy 2 .16 Seismic Anisotropy of the Deep Earth from a Mineral and Rock Physics Perspective. Treatise on Geophysics 2, 437–491.

Manatschal. G, Sauter D., Karpoff A.M., Masini, E., Mohn, G., Lagabrielle, Y., 2011. The Chenaillet Ophiolite in the French/Italian Alps: An ancient analogue for an Oceanic Core Complex? Lithos 124, 169-184.

Marroni, M., Molli, G., Montanini, A., Tribuzio, R., 1998, The association of continental crust rocks with ophiolites in the Northern Apennines (Italy): implications for the continent-ocean transition in the Western Tethys. Tectonophysics 292, 43-66.

Marroni, M., Pandolfi L. 2007. The architecture of an incipient oceanic basin: a tentative reconstruction of the Jurassic Liguria-Piemonte basin along the Northern Apennines–Alpine Corsica transect. International Journal of Earth Sciences 96, 1059-1078.

Marroni, M., Molli, G., Ottria. G., Pandolfi, L., 2001. Tectono-sedimentary evolution of the

ACCEPTED MANUSCRIPT

External Liguride units (Northern Apennine, Italy): Insights in the precollisional history of a fossil ocean–continent transition zone. Geodinamica Acta 14, 307–320

Marroni, M., Meneghini, F., Pandolfi, L., 2010. Anatomy of the Ligure- Piemontese subduction system: evidences from Late Cretaceous-Middle Eocene convergence-related deposits from Northern Apennines (Italy). International Geology Review 10-12, 1160-1192.

Massa, G., Musumeci., G., Mazzarini, F., Pieruccioni, D., 2016. Coexistence of contractional and extensional tectonics during the northern Apennines orogeny: the late Miocene out-of-sequence thrust in the Elba Island nappe stack. Geological Journal early view.

Mehl, L., Hirth, G., 2008. Plagioclase preferred orientation in layered mylonites: Evaluation of flow laws for the lower crust, Journal of Geophysics Research 113, B05202.

Mellini M., Rumori, C., Viti, C., 2005. Hydrothermally reset magmatic spinels in retrograde serpentinites: formation of ‘‘ferritchromit’’ rims and chlorite aureoles. Contributions Mineralogy and Petrology 149, 266–275.

Miranda, E., John B., 2010. Strain localization along the Atlantis Bank oceanic detachment fault system, Southwest Indian Ridge, Geochemistry, Geophysics, Geosystems 11, Q04002.

Molli, G., 1996. Pre-orogenic tectonic framework of the northern Apennine ophiolites. Eclogae Geologicae Helvetiae 89, 163-180.

Montanini, A., Tribuzio, R., Thirlwall, M., 2012. Garnet clinopyroxenite layers from the mantle sequences of the Northern Apennine ophiolites (Italy): evidence for recycling of crustal material. Earth and Planetary Science Letters 351, 171–181.

Nicholas A., Mashi, A., Boudier, F., Jousselin, D., Muceku, B., 2017. Mylonites in ophiolite of Mirdita (Albania): Oceanic detachment shear zone. Geosphere, 13, 136-154.

Ohara, Y., Fujioka, K., Ishii, T., Yurimoto H., 2003. Peridotites and gabbros from the Parece Vela backarc basin: Unique tectonic window in an extinct backarc spreading ridge. Geochemistry, Geophysics, Geosystems 4, 8611.

ACCEPTED MANUSCRIPT

Passchier, C.W., Trouw, R.A.J., 2006. Micro-tectonics, 2nd ed. Springer-Verlag, Berlin, Heidelberg.

Perrin, M., 1975. L'Ile d'Elbe et la limite Alpes-Apennins: données sur la structure geologique et l'evolution tectogenitique de l'Elbe alpine et de l'Elbe apennine. Bollettino della Società Geologica Italiana 94, 1929–55.

Piazolo, S., Austrheim, H., and Whitehouse, M. (2012) Brittle-ductile microfabrics in naturally deformed zircon: Deformation mechanisms and consequences for U-Pb dating. American Mineralogist, 97, 1544–1563.

Piccardo, G.B., Padovano, M., Guarnieri, L., 2014. The Ligurian Tethys: mantle processes and geodynamics. Earth Sciences Review 138, 409–434.

Raggi, G., Squarci, P. Taffi, L., 1965. Considerazioni stratigrafico-tettoniche sul Flysch dell'Isola d'Elba. Bollettino della Società Geologica Italiana 84, 1–14.

Rampone, E., Hofmann, A. W., Piccardo, G. B., Vannucci, R., Bottazzi, P., Ottolini, L., 1995. Petrology, mineral and isotope geochemistry of the External Liguride peridotites (Northern Apennine, Italy). Journal of Petrology 36, 81–105.

Ray, D., Mevel, C., Banerijee, R., 2009. Hydrothermal alteration studies of gabbros from Northern Central Indian Ridge and their geodynamic implications. Journal of Earth System Sciences 118 659-676.

Reutter, K.J., Spohn, A., 1982. The position of the West-Elba ophiolites within the tectonic framework of the Apennines. Ofioliti 2/3, 467-478.

Rossetti, F., Tecce, F., Billi, A., Brilli, M., 2007, Patterns of fluid flow in the contact aureole of the Late Miocene Monte Capanne pluton (Elba Island, Italy): The role of structures and rheology. Contribution Mineralogy and Petrology 153, 743–760.

Rubatto, D., and Hermann, J., 2003. Zircon formation during fluid circulation in eclogites (Monviso, Western Alps): implications for Zr and Hf budget in subduction zones. Geochimica et Cosmochimica Acta, 67, 2173-2187.

ACCEPTED MANUSCRIPT

Saccani, E., Principi, G., 2016. Petrological and tectono-magmatic significance of ophiolitic basalts from the Elba Island within the Alpine Corsica-Northern Apennine system. Mineralogy and Petrology,, 110, 713-730.

Sanfilippo, A., Tribuzio, R., 2011. Melt transport and deformation history in a "non-volcanic" ophiolitic section (Northern Apennine, Italy): implications for crustal accretion at slow spreading settings. Geochemistry, Geophysics, Geosystems Q0AG04.

Siegesmund, S., Helming, K., Kruse, R. 1994. Complete Texture Analysis of a Deformed Amphibolite: Comparison between Neutron, Diffraction and U-Stage Data. Journal of Structural Geology 16, 131–42.

Soda, Y., Morishita. T., Tamura, A., Arai, S., 2010. Phlogopite-bearing peridotite from 25°S oceanic core complex near Rodriguez Triple Junction. Goldschmidt Conference Abstracts 2904.

Tartarotti P., Vaggelli G., 1994. Mantle peridotites and cumulates from the Elba Island ophiolites: fragments of the oceanic mantle-crust transition zone. Ofioliti 19, 319-325.

Timms, N.E., Kinny, P., and Reddy, S.M. (2006) Enhanced diffusion of uranium and thorium linked to crystal plasticity in zircon. Geochemical Transactions, 7, 10.

Toomey, D.R., Purdy, G.M., Solomon, S.C., 1988. Microearthquakes beneath the m edian valley of the Mid-Atlantic ridge near 23°N: Tomography and tectonics. Journal of Geo-physical Research, 93, 9093– 9112.

Tremblay, A., Meshi, A., Bédard, J.H., 2009. Oceanic core complexes and ancient oceanic lithosphere: insights from Iapetan and Tethyan ophiolites (Canada and Albania). Tectonophysics 473, 36–52.

Tribuzio, R., Tiepolo, M., Vannucci, R., 2000. Evolution of gabbroic rocks from the Northern Apennine ophiolites (Italy): comparison with the lower oceanic crust from modern slow-spreading ridges. In: Dilek, Y., Moores, E.M., Elthon, D., Nicolas, A. (Eds.), Ophiolites and Oceanic Crust: New Insights from Field Studies and the Oceanic Drilling Program. Geological

ACCEPTED MANUSCRIPT

Society of America Special Papers 349, 129–138.

Tribuzio R., Riccardi M.P., Ottolini L., 1995. Trace elements in high temperature deformed gabbros from East Ligurian ophiolites (northern Apennines. Italy): Constraints on the origin of syn-deformation fluids. Journal of Metamorphic Geology,13, 367-377.

Tribuzio, R., Garzetti, F., Corfu F., Tiepolo, M., Renna, M.R., 2015. U–Pb zircon geochronology of the Ligurian ophiolites (Northern Apennine, Italy): Implications for continental breakup to slow seafloor spreading. Tectonophysics 666, 220-243.

Tribuzio, R., Renna, M.R., Dallai, L., Zanetti, A., 2014. The magmatic-hydrothermal transition in the lower oceanic crust: clues from the Ligurian ophiolites, Italy. Geochimica Cosmochimica Acta 130, 188–211.

Tribuzio, R., Thirwall, M.F., Vannucci, R., 2004. Origin of the gabbro–peridotite association from the Northern Apennine ophiolites (Italy). Journal of Petrology 45, 1109–1124.

Tucholke, B.E., Lin, J., Kleinrock, M.C., 1998. Megamullions and mullion structure defining oceanic metamorphic core complexes on the Mid-Atlantic Ridge, Journal of Geophysics Research 103(B5), 9857–9866.

Vauchez, A., Tommasi, A., Mainprice, D., 2012. Faults (shear zones) in the Earth's mantle. Tectonophysics 558, 1-27.

Warren, J.M., Hirth, G., Kelemen, P.B., 2008. Evolution of olivine lattice preferred orientation during simple shear in the mantle. Earth and Planetary Science Letters 272, 501–512.

Westerman, D.S., Dini, A., Innocenti, F., and Rocchi, S., 2004, Rise and fall of a nested Christmas-tree laccolith complex, Elba Island, Italy. In: Breitkreuz, C., Petford, N., eds., Physical geology of high-level magmatic systems. Geological Society of London Special Publication 234, 195–213.

Zhang, X.L., Hu, L., Ji, M., Liu, J.L., Song, H.L., 2013. Microstructures and deformation mechanisms of hornblende in Guandi complex, the Western Hills, Beijing. Science China Earth Sciences 56, 1510–1518.

ACCEPTED MANUSCRIPT

Zucali, M., Fontana, E., Panseri, M., Tartarotti, P., Capelli, S., Ouladdiaf, B., 2014. Submarine lava flow direction revealed by neutron diffraction analysis in mineral lattice orientation. Geochemistry, Geophysics, Geosystems 15, 765–780.

ACCEPTED MANUSCRIPT

ACCEPTED MANUSCRIPT

Figure Captions

Fig. 1. Ophiolitic units in Northern Apennines, Corsica Island and western Alps.

Fig. 2. Geological sketch map of Elba Island and location of study area.

Fig. 3. Schematic geological cross section of the Cotoncello Shear Zone (CSZ). The stereographic projections of the main structures are indicated (Schmidt projection, lower hemisphere), as well as the location of studied samples and the pictures showed in Figs. 5 and 14.

Fig. 4. Summary of the fabrics documented at meso and microscopic scale in gabbros and peridotites in the CSZ. See text for further details.

Fig. 5. Field evidences of the Cotoncello Shear Zone (see Fig. 3 for location). (a) Lens of proto-tectonite peridotites (proto-tect) wrapped by tectonite peridotite foliation (Stect). (b) Tectonites peridotite (Stect) partly overprinted by amphibole-bearing mylonitic foliation (Amp-my). Black rectangles indicate the location of microphotographs shown in Figs. 7c and 10c. Sub-millimeter veins of fibrous serpentine cross cut the amphibole-bearing mylonitic foliation (white arrow). (c) Lenses of metagabbro (m-g) preserved within mylonite gabbro (Pl: plagioclase; Smy: mylonitic foliation). The location of photomicrographs shown in Fig. 10a, b is indicated. The picture represents a vertical surface and it is rotate 90° anticlockwise. (d) Network of ultramylonites in gabbros. (m-g: meta-gabbro; Su-my: ultramylonitic foliation). The location of Fig. 10c is indicated. The picture represents a vertical surface and it is rotate 90° anticlockwise. (e) Meter-thick localized shear zone in tectonite peridotites in the eastern portion of the CSZ (Amph-Sm: amphibole-bearing foliation). (f) Detail of the localized shear zone in gabbros. Decimeter-sized lens of gabbro showing

ACCEPTED MANUSCRIPT

an internal mylonitic and ultramylonitic foliation (Smy) oriented at high-angle to the external fine-grained amphibole-bearing foliation (Amph-Sm).

Fig. 6. Geometrical relations between Miocene intrusive rocks and CSZ. See Fig. 3 for pictures location. (a) Portoferraio porphyry limiting the eastern boundary of the CSZ. A sketch showing the geometrical relation between tectonite peridotite (Stect) and sub-solidus magmatic foliation (Smag) in porphyry is also indicated. (b) Cross-cutting relationships between the meter-thick undeformed granite dyke located in the central portion of the CSZ and the mylonite peridotite (Smy: mylonitic foliation). (c) Enclaves of mylonite gabbros within the undeformed meter-thick granite dyke in the central portion of the CSZ (Smy: mylonitic foliation).

Fig. 7. U-Pb Zr geochronology. (a) Concordia diagram and (b) U-Pb concordant data from the selected zircons.

Fig. 8. Photomicrographs of microstructures in proto-tectonite (PF1) and tectonite peridotites (PF2). (a) Weak isoriented olivine crystals (Ol) with amoeboid boundaries (white arrow) and sub- and new-grains (white and black circle, respectively) in prototectonites (cross-polarized light, XPL). Triple junctions (black arrow) may indicate the occurrence of to grain growth/annealing processes. Isoriented acicular Mg-hornblende (Mg-Hbl) crystals (PF4) overprint the olivine and orthopyroxene (Opx) crystals. (b) White dash lines delimit relicts of olivine (Ol) –ribbons characterizing the tectonite fabric (PF2). This fabric is overprinted by mylonite peridotite (PF3) and by shear planes (yellow lines) marked by elongated spinel (Sp) and fine-grained olivine crystals, which define sigma-type olivine porphyroclast. Amphibole-bearing layers (Amph-Sm; PF3) overprint both tectonite (Stect; PF1) and mylonite (Smy: PF2) foliations; black arrow: antophillite - gedrite amphibole related to the contact metamorphism occurred during the Mt. Capanne pluton emplacement. Plane-polarized light (PPL). (c) Olivine (Ol) ribbon (delimited by white lines, PF2)

ACCEPTED MANUSCRIPT

preserved within mylonite peridotite (PF3; Smy: mylonitic foliation; PF3) (PPL). Amphibole–bearing foliation (Amph-Sm; PF4) cross cuts at low-angle the olivine-ribbon and the mylonitic foliation. The location of Fig. 7d is indicated. Sp: spinel: Mg-Ilm: Mg-rich Ilmenite; Ilm: ilmenite. (d) Backscattering SEM image showing detail of Fig. 7c. Ol: olivine; Sp: spinel; Gd: gedrite; Amph: amphibole; Ilm: ilmenite.

Fig. 9. Photomicrographs of mylonite peridotite microstructures (PF3). (a) Clinopyroxene (Cpx) porphyroclast (partly replaced by amphibole) surrounded by a fine-grained matrix of olivine (Ol), orthopyroxene, spinel and ilmenite. Cross-polarised light (XPL). Below the CPx, an Ol-ribbon relicts of PF2, lies parallel to the mylonitic foliation (Smy). In the upper portion of the photomicrograph, the Smy is overprinted by amphibole–bearing foliation (Amph-Sm; PF4). (b) Aggregate of clinopyroxene (CPx) crystals enveloped by the mylonitic foliation (Smy) and by thin olivine-ribbons (white lines) (XPL). The biggest clinopyroxene show olivine (Ol) lamellae and olivine embayments. The upper strain cap is marked by strongly elongated olivine crystals affected by undulatory extinction. Amph-Sm: amphibole-bearing foliation. The location of Fig. 8c is indicated. (c) Backscattering SEM image of a fine-grained domain located in the strain shadow of the clinopyroxene porphyroclast (CPx) in Fig. 8b. Ol: olivine; Pl: plagioclase. (d) Clinopyroxene (CPx) porphyroclast enveloped by the amphibole-bearing foliation (Amph-Sm; PF4) (XPL). Smy: mylonite foliation; Ol: olivine; ngOl: olivine new grain. The location of Fig. 8e is indicated. (e) Backscattering SEM image of a fine-grained domain located in the rim of the clinopyroxene porphyroclast (CPx) in Fig. 8d. Ol: olivine; OPx: orthopyroxene; Chl: chlorite.

Fig. 10. Microstructures in gabbros. (a) Medium to coarse-grained plagioclase (Pl) and pyroxene (Px) euhedral crystals showing evidence of weak dynamic recrystallization (fabric GF1) Cross-polarized light (XPL). (b) Mylonite fabric (GF2) marked by flattened aggregates of isoriented pyroxene (Px) and plagioclase (Pl). The porphyroclasts are wrapped by the mylonitic foliation (Sm)

ACCEPTED MANUSCRIPT

overprinted by the lower temperature amphibole-bearing foliation (Amph-Sm) (XPL). (c) Ultramylonite fabric (GF2) is marked by fine-grained layers of plagioclase (Pl) and pyroxene (Px) + plagioclase (±titanite: Ti). Phl: phlogopite; Smy: mylonite foliation. Plane-polarized light. (d) Backscattering SEM image of ultramylonite. See Fig. 9c for location. Pl: plagioclase; Px: pyroxene; Phl: phlogopite.

Fig. 11. Phlogopite metamorphic event. (a) Phlogopite (Phl) crystals overprinted by later amphibole crystal (Amph) of PF4. Cross-polarized light (XPL). (b) Backscattering SEM image of phlogopite (Phl) crystals truncated by the amphibole-bearing foliation (Amph-Sm) of PF4. Pl: plagioclase; Ol: olivine; Mg-Hbl: Mg-hornblende; Chl: chlorite; Stect: tectonite foliation (PF2); Note the euhedral gedrite crystals (Gd) grew on both Pl, Phl and on Amph-Sm. (c) Vein of phlogopite grown orthogonally respect to the mylonitic foliation (Smy; GF2). Pl: plagioclase; Plane-polarized light. (d) Syn-kinematic phlogopite (Phl) filling the offset of bookshelf structures in a plagioclase (Pl) (XPL). Px: pyroxene; Smy: mylonitic foliation of GF2.

Fig. 12. Microstructures and mineral composition of amphiboles related to fabric PF4-GF3. (a) Chemical composition of amphiboles. (b) Plagioclase (Pl) crystal deformed during the ductile mylonitic event (GF2) disrupted by microfaulting. Isoriented syn-kinematic amphibole (Amph) crystals grew between the two fragments (PPL). Amph-Sm: Amphibole-bearing foliation; Chl: chlorite; Px: pyroxene. (c) C'-type shear bands highlighted by fine-grained amphibole crystals (XPL). Ol: olivine; Amph- Sm: amphibole-bearing mylonitic foliation; C: shear plane; S: mylonitic foliation.

Fig. 13. LPO Pole figures for amphibole and olivine in FP2 and FP3 peridotites from the CSZ (samples COT14, COT16 and COT18). X-Y-Z mesoscopic fabric axes are shown schematically as reference for pole figures. Crystallographic relations for amphibole monoclinic (2^{nd} setting) and

ACCEPTED MANUSCRIPT

olivine orthorhombic are also shown together with relations between normal to crystallographic planes and crystallographic axes.

Fig. 14. Cartoon showing the evolution of the Tethyan Oceanic Core Complex using the information collected in the CSZ. See text for further explanations and discussions.

Fig. 15. Sketch of oceanic core complex at a slow spreading ridge with domain of hydrothermal circulation. The zone of active serpentinization is characterized by decrease in density and lower P waves velocity (right). Hypothetical location of fabrics documented in the CSZ is also shown.

ACCEPTED MANUSCRIPT

ACCEPTED MANUSCRIPT

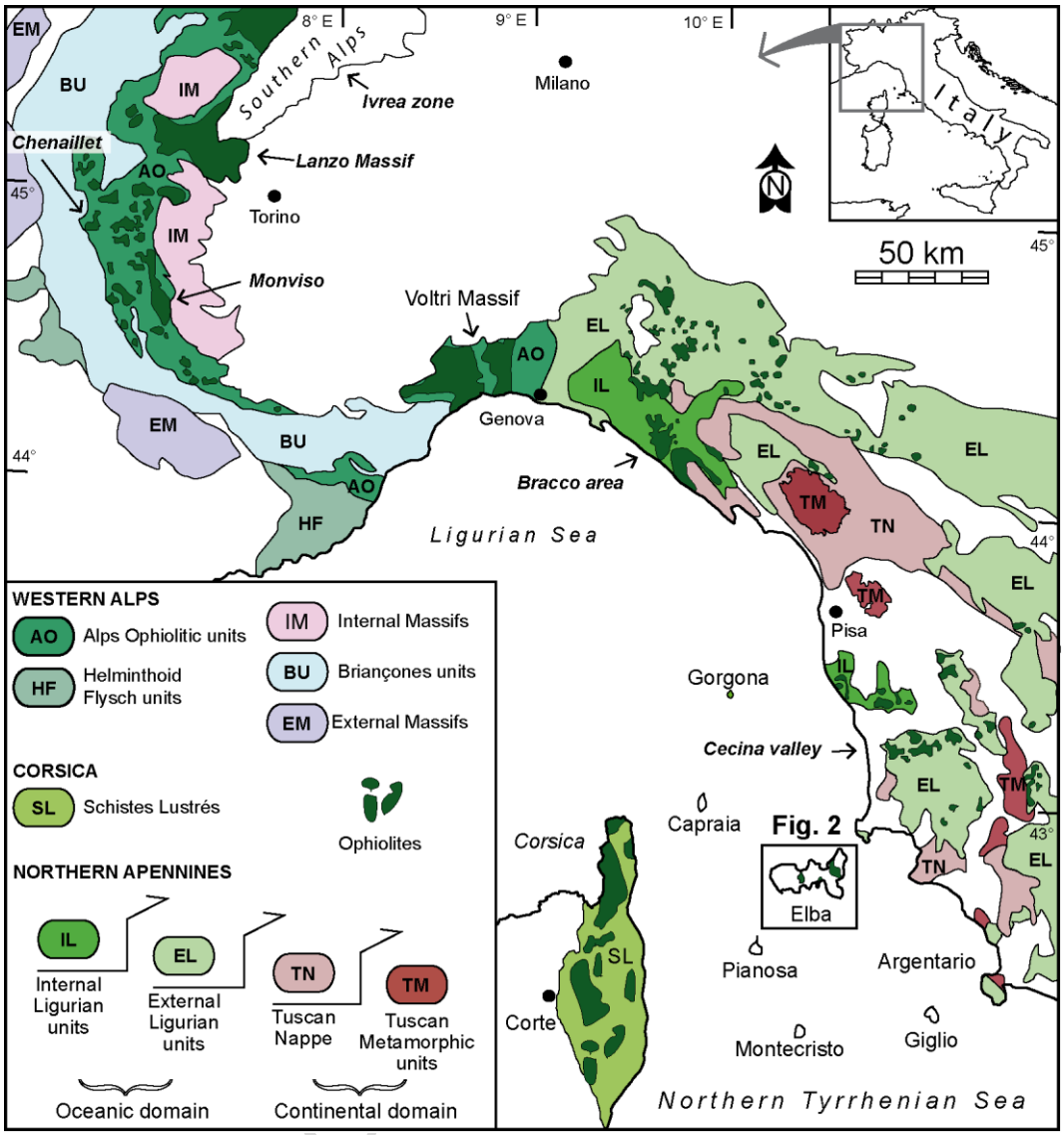

Figure 1

ACCEPTED MANUSCRIPT

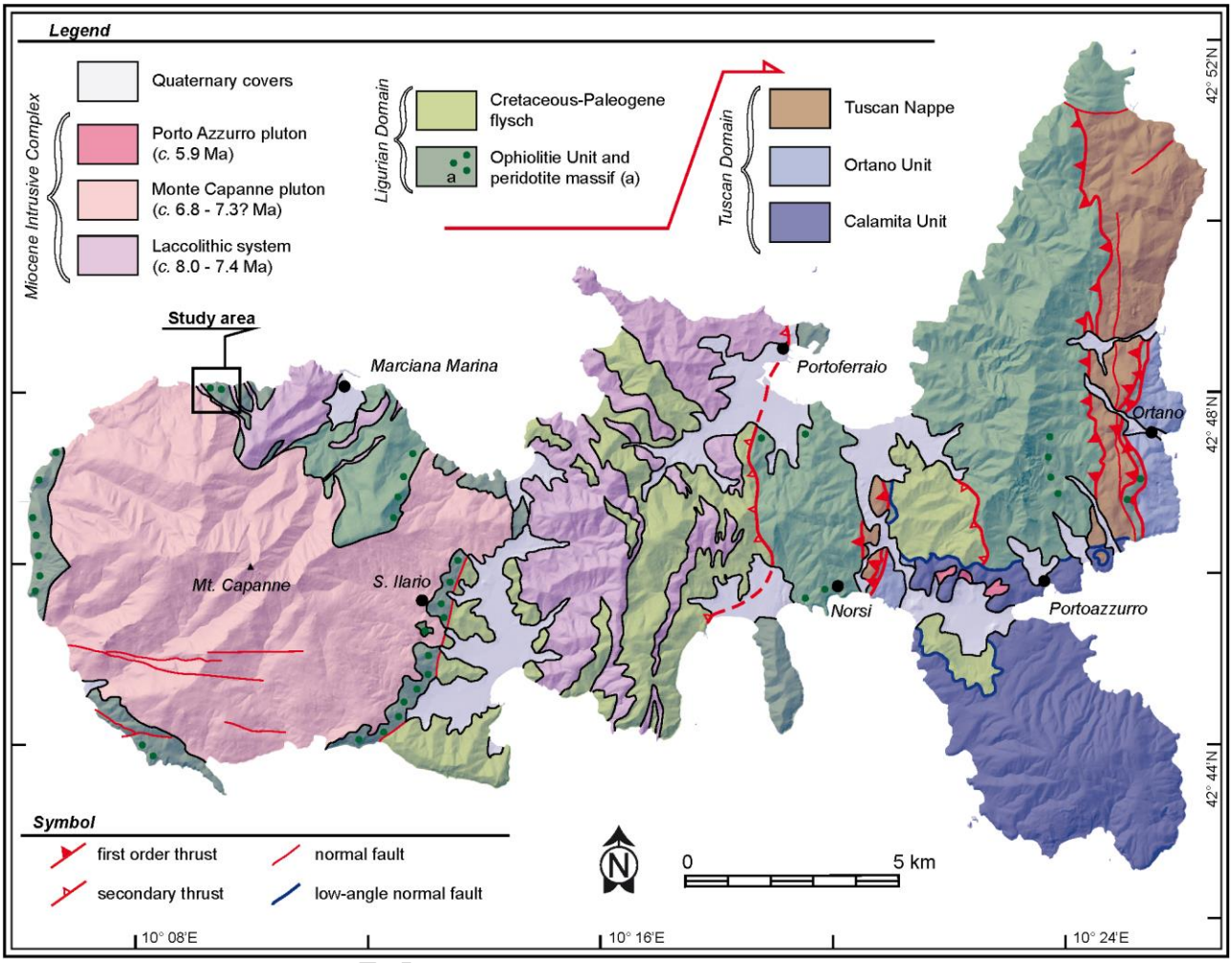

Figure 2

ACCEPTED MANUSCRIPT

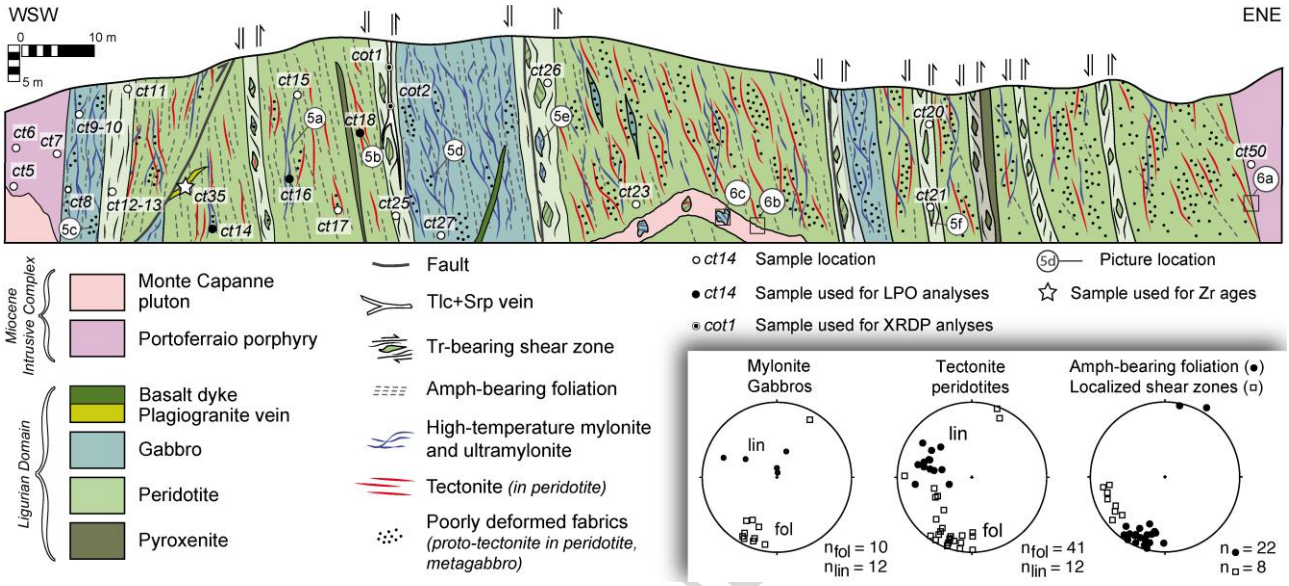

Figure 3

ACCEPTED MANUSCRIPT

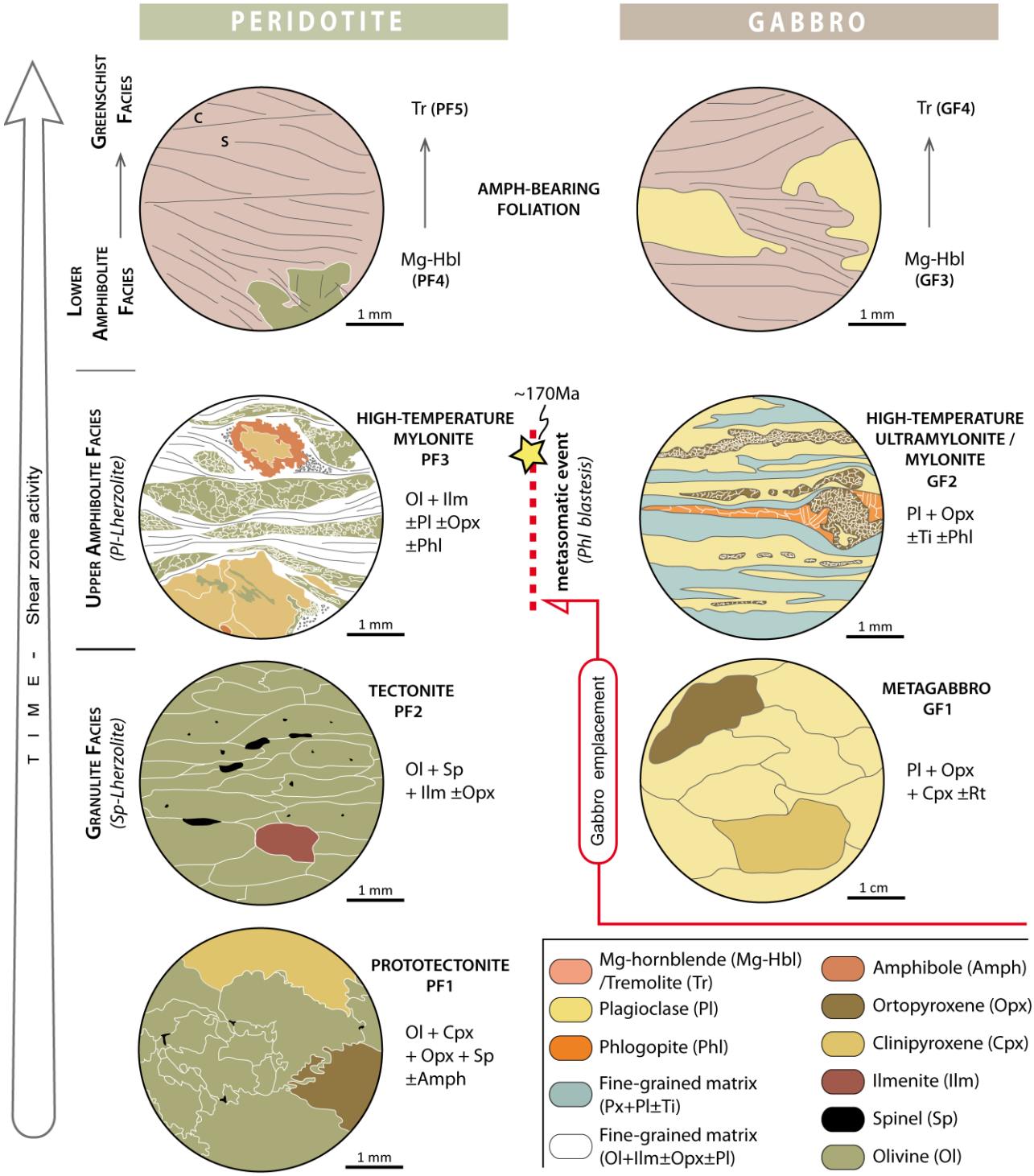

Figure 4

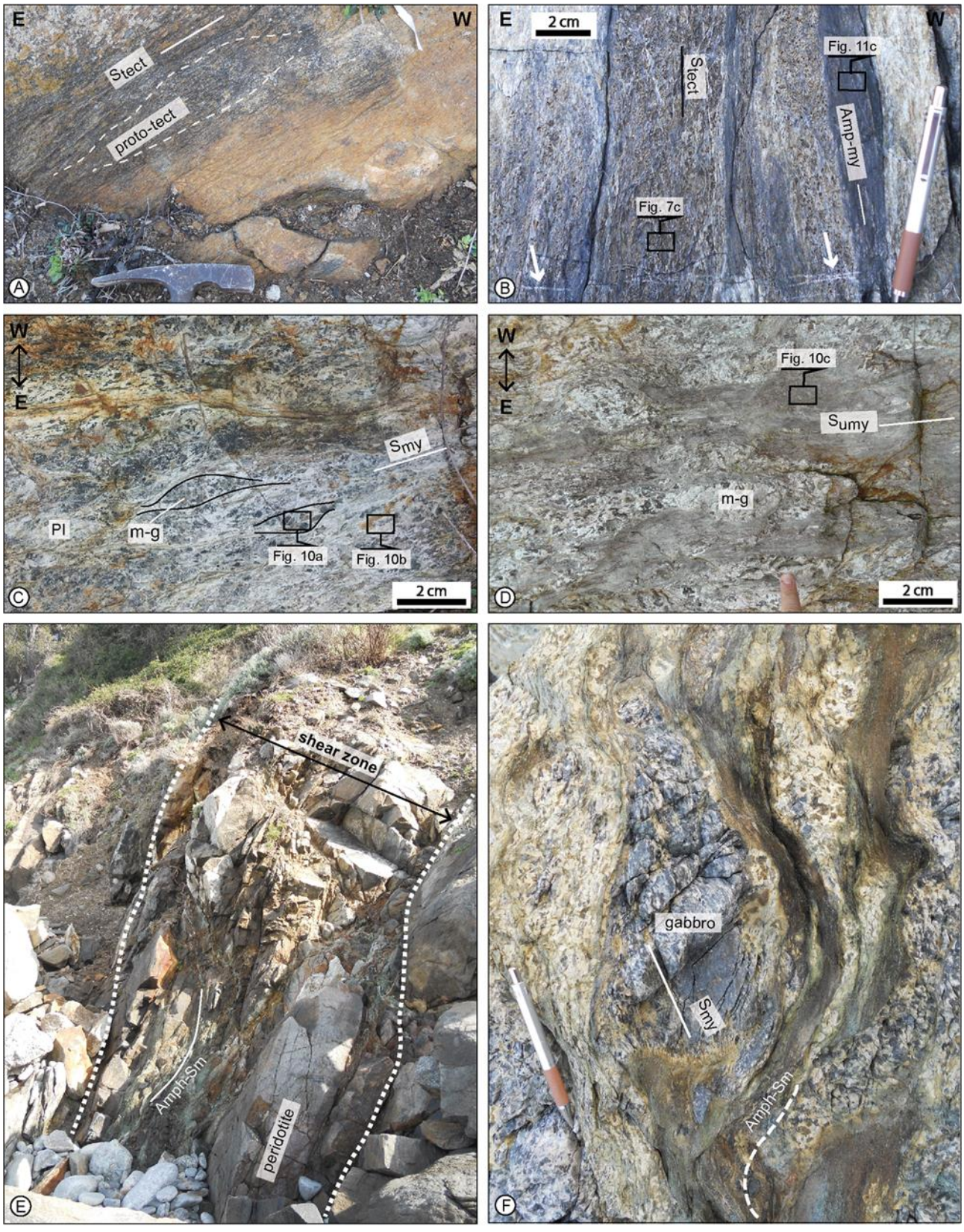
E
W
Stect
proto-tect
A
E
2 cm
W
Stect
Fig. 11c
Amp-my
Fig. 7c
B
W
E
Smy
Pl
m-g
Fig. 10a
Fig. 10b
2 cm
C
W
E
Fig. 10c
Sumy
m-g
2 cm
D
shear zone
Amph-Sm
peridotite
E
gabbro
Smy
Amph-Sm
F

Figure 5

ACCEPTED MANUSCRIPT

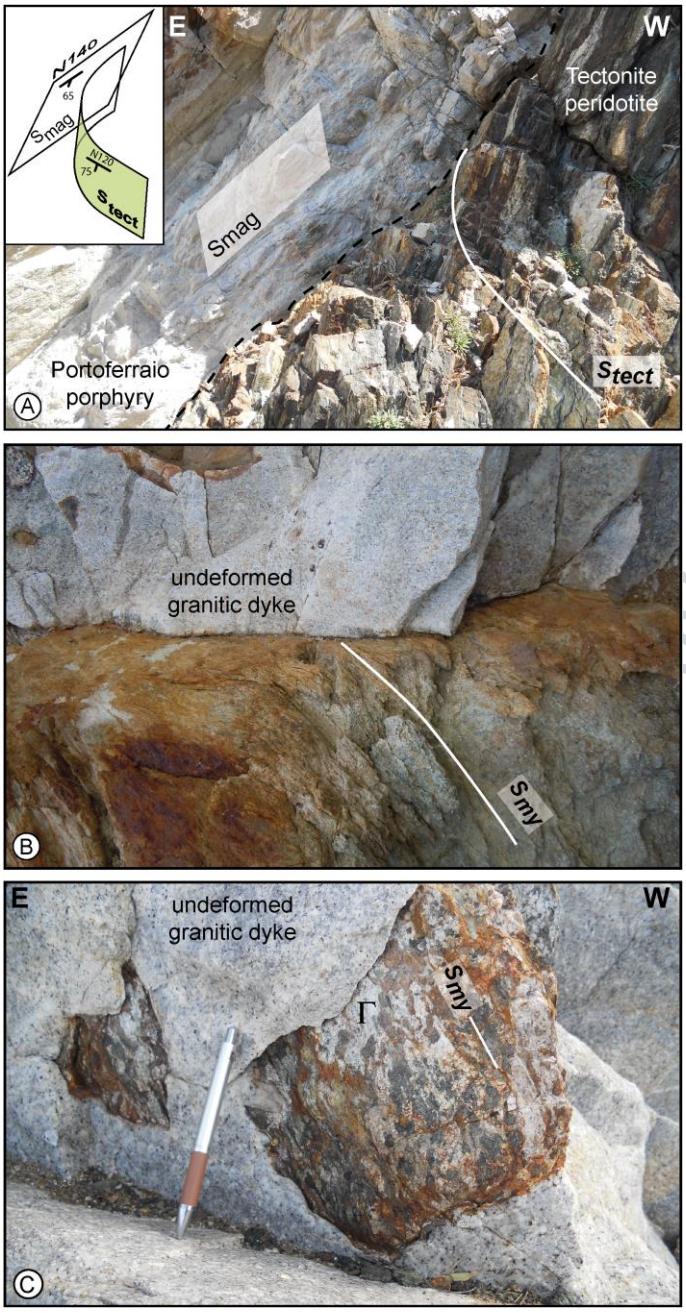

Figure 6

ACCEPTED MANUSCRIPT

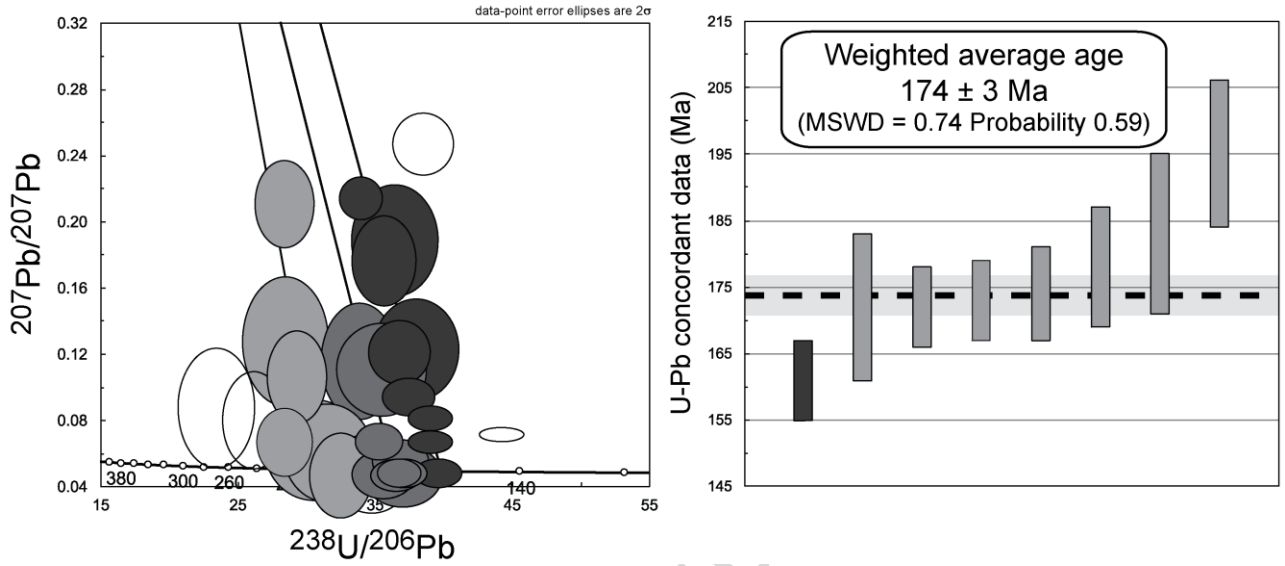

Figure 7

ACCEPTED MANUSCRIPT

ACCEPTED MANUSCRIPT

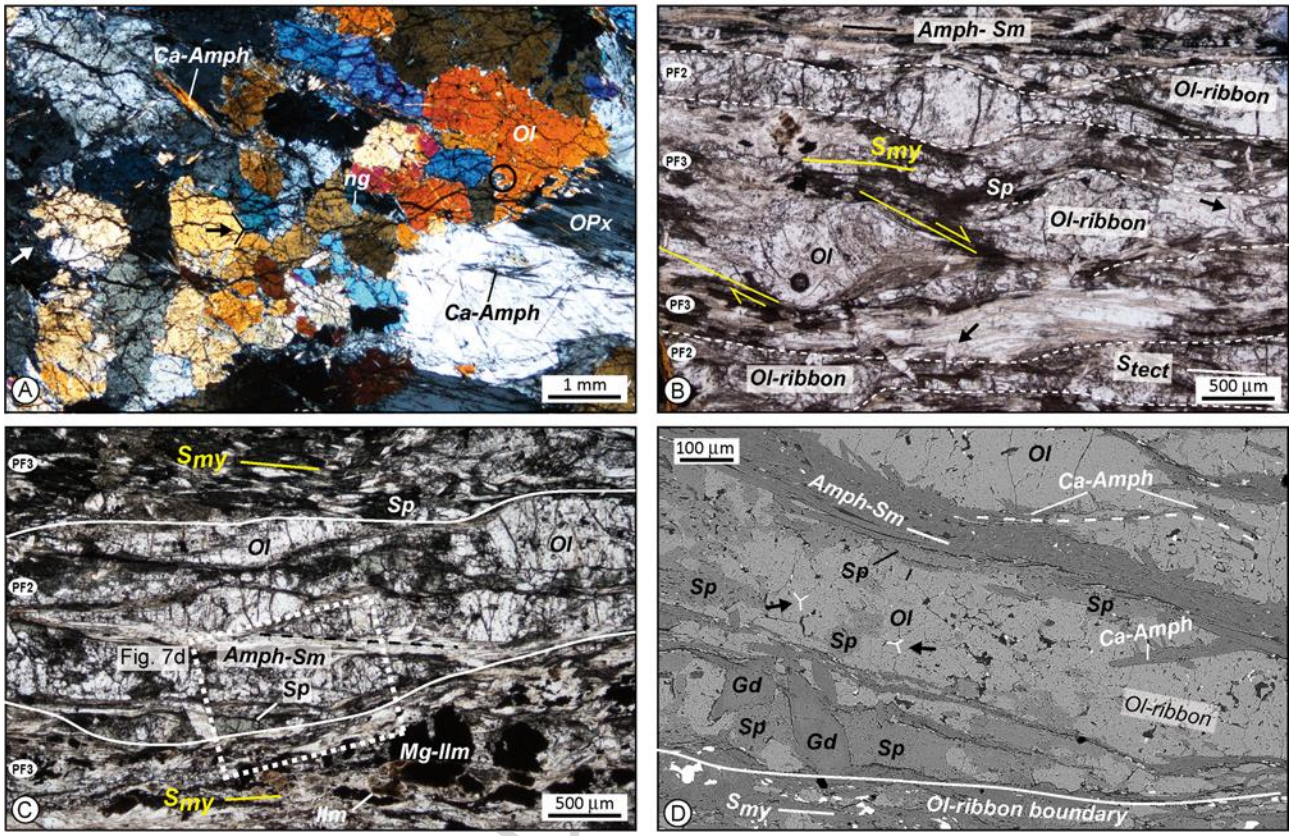

Figure 8

ACCEPTED

ACCEPTED MANUSCRIPT

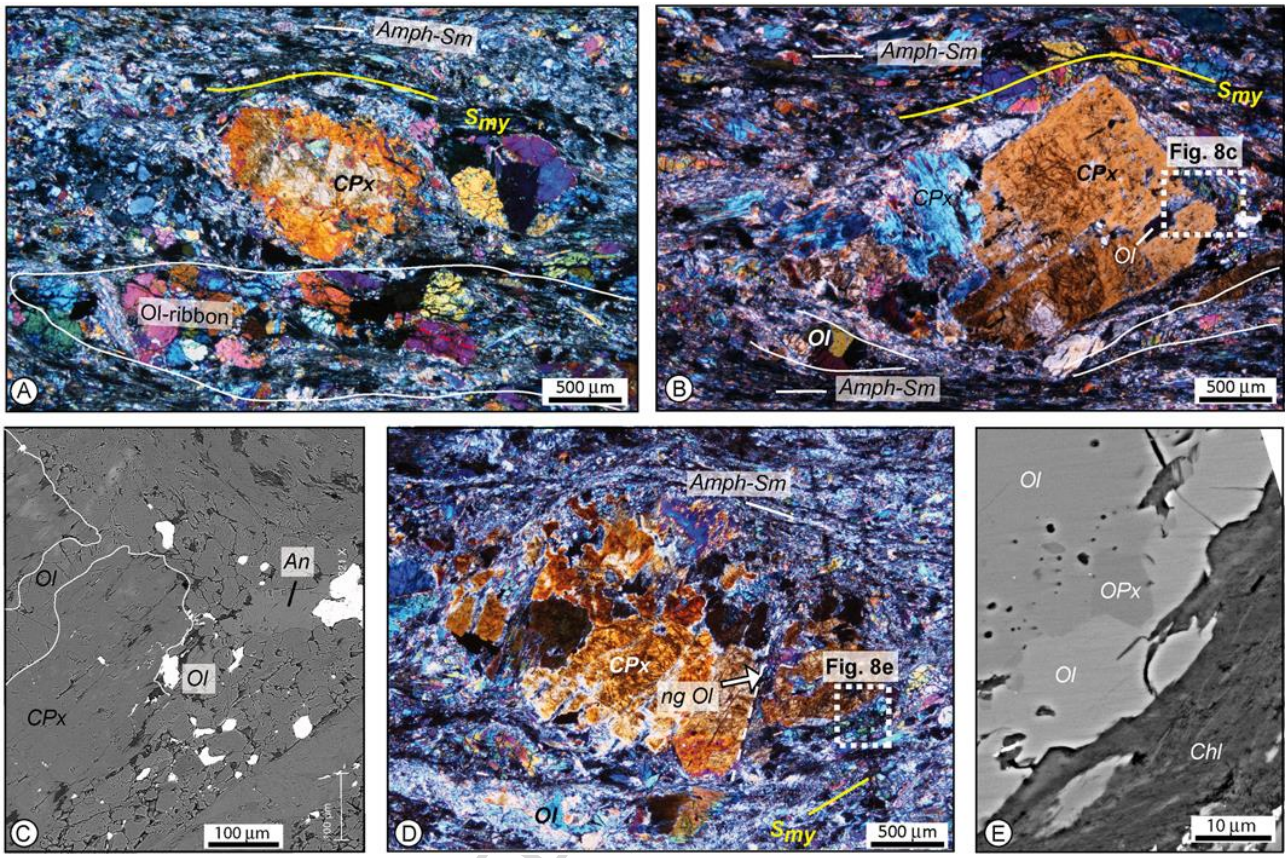

Figure 9

ACCEPTED

ACCEPTED MANUSCRIPT

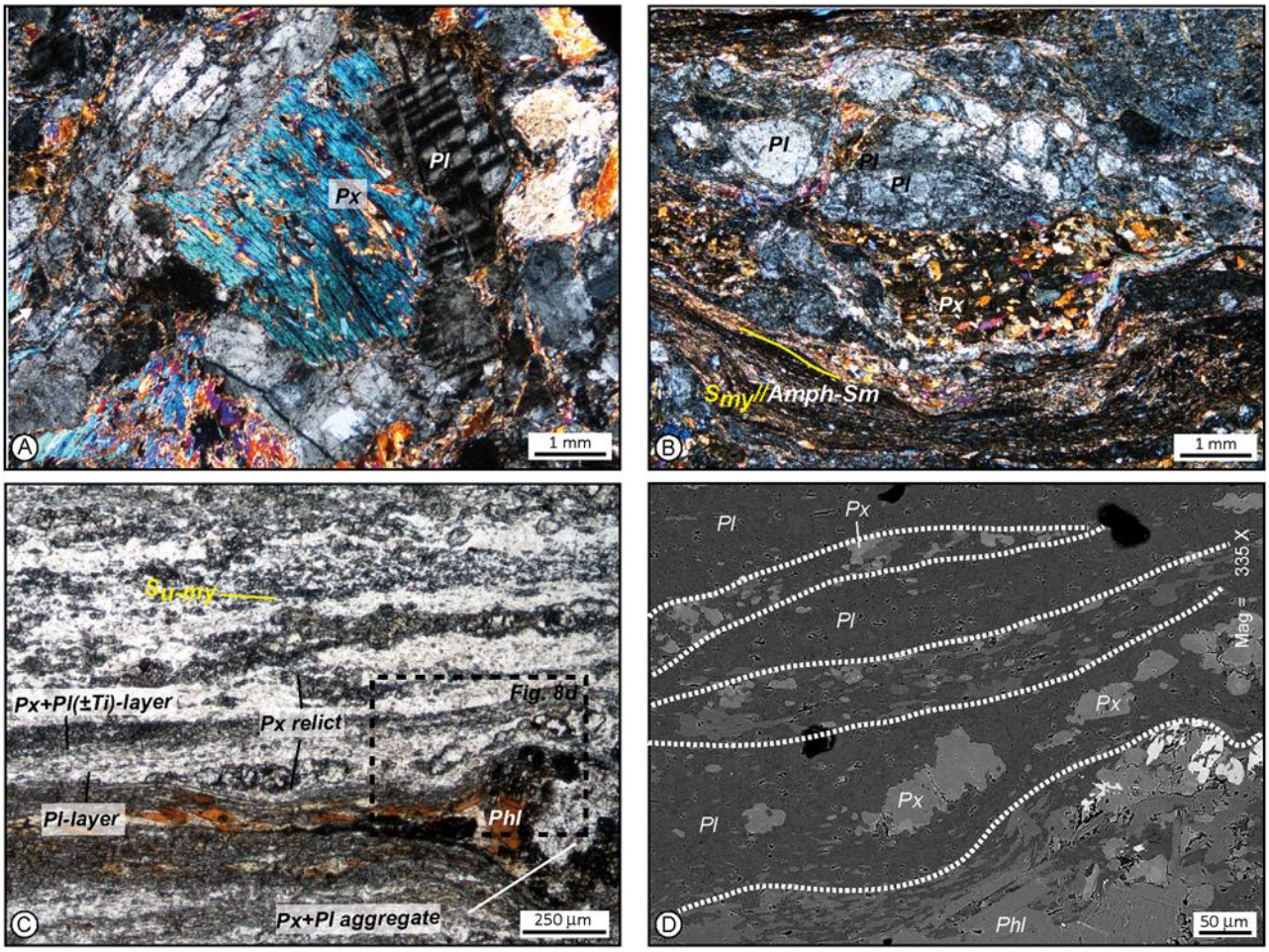

Figure 10

ACCEPTED MANUSCRIPT

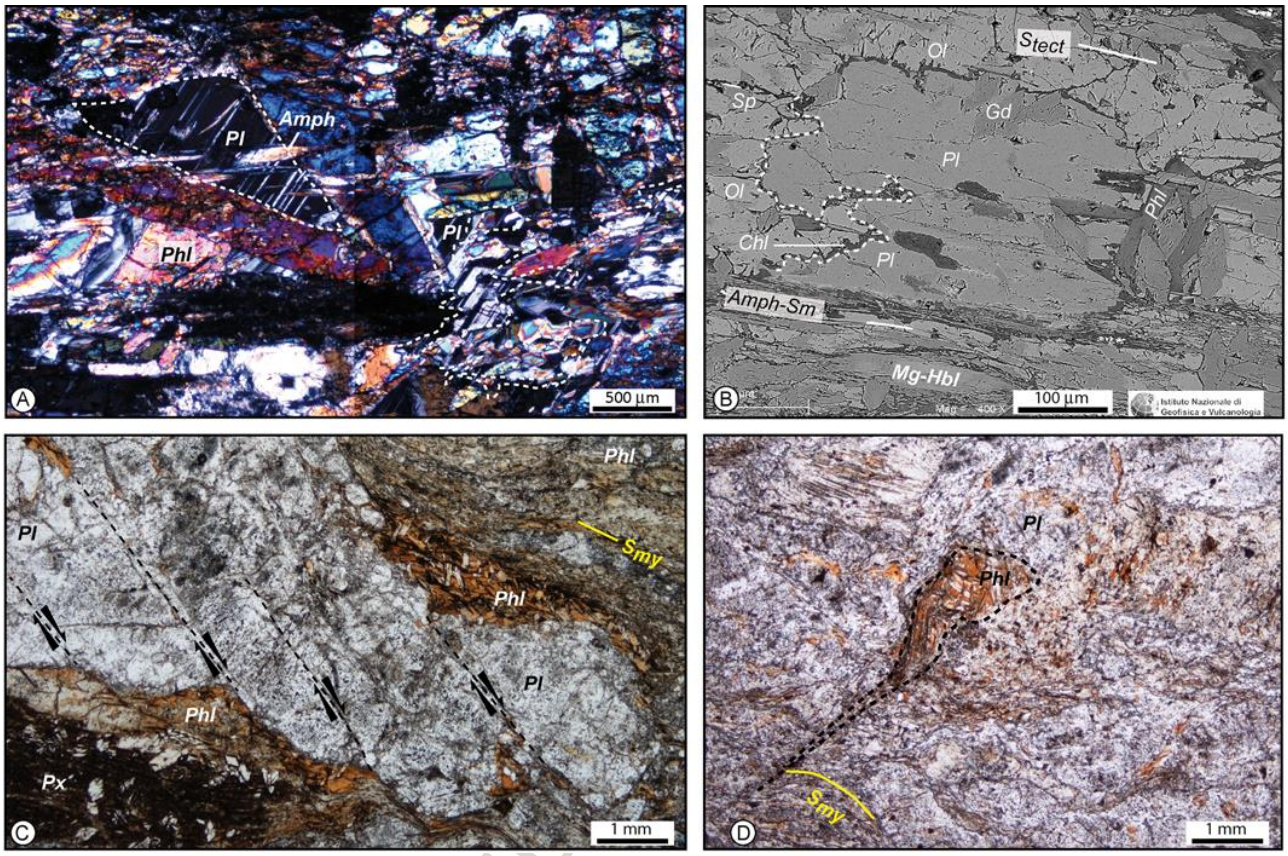

Figure 11

ACCEPTED

ACCEPTED MANUSCRIPT

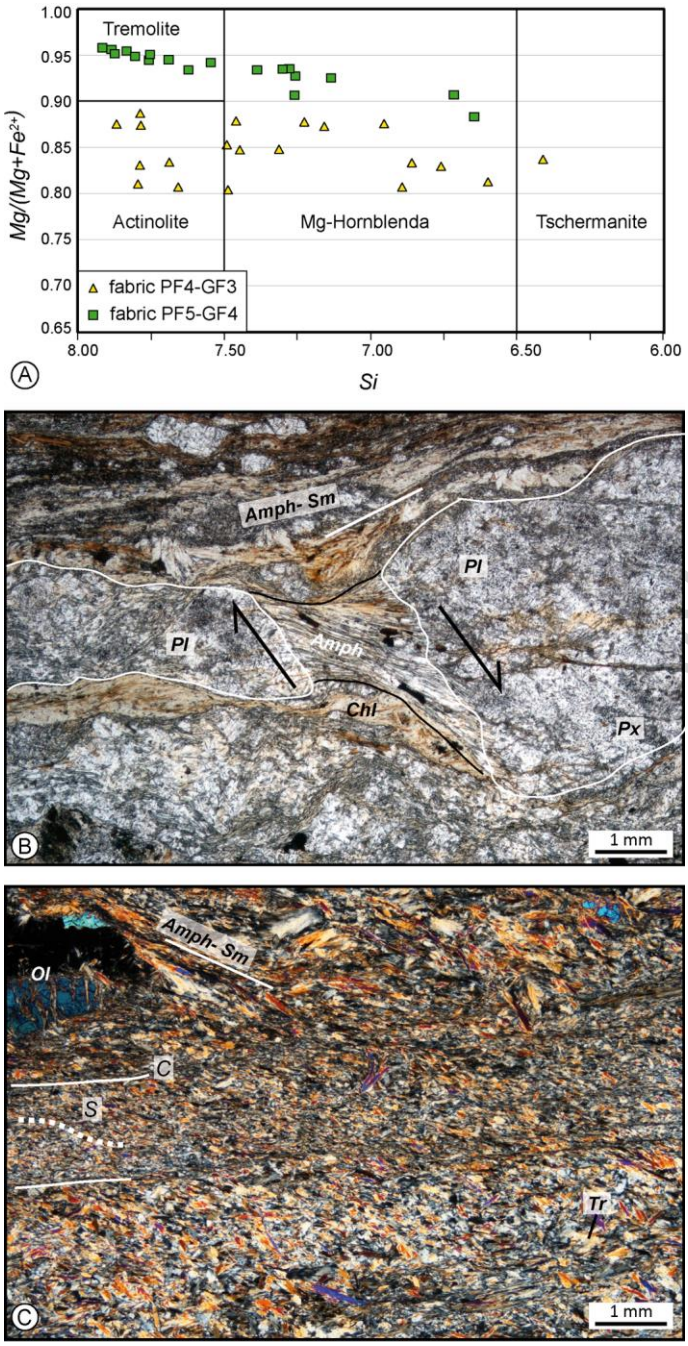

Figure 12

ACCEPTED MANUSCRIPT

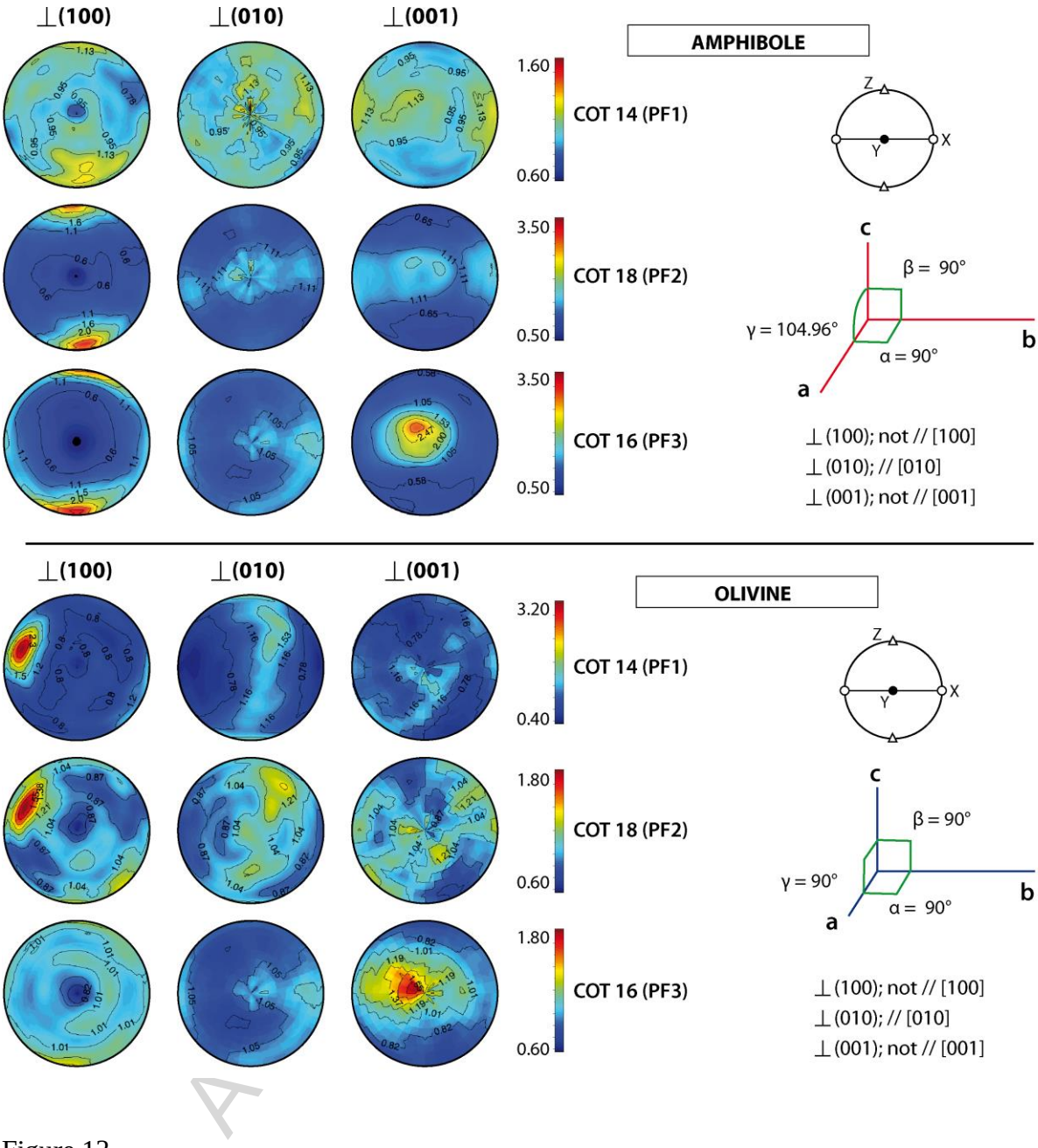

Figure 13

ACCEPTED MANUSCRIPT

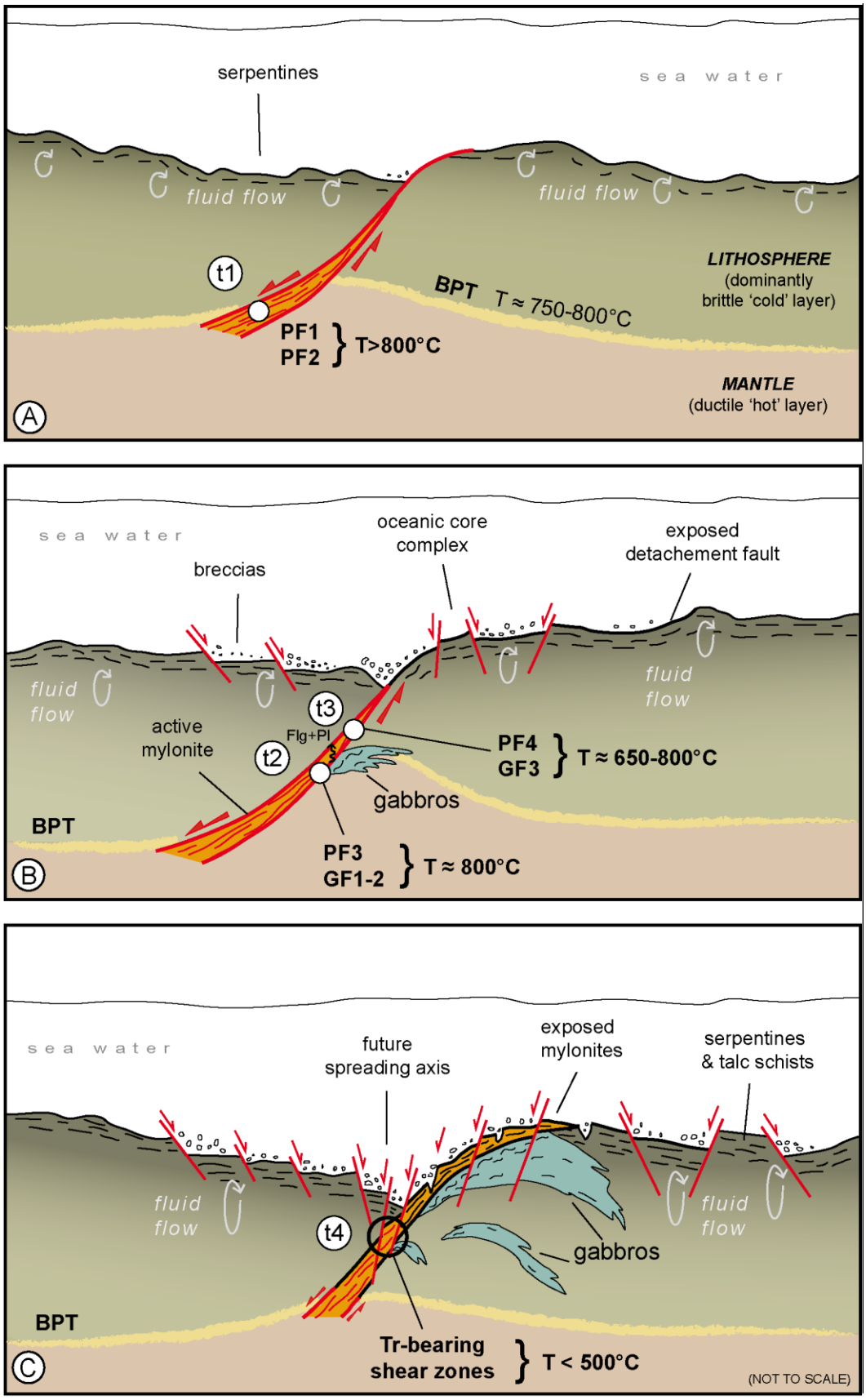

Figure 14

ACCEPTED MANUSCRIPT

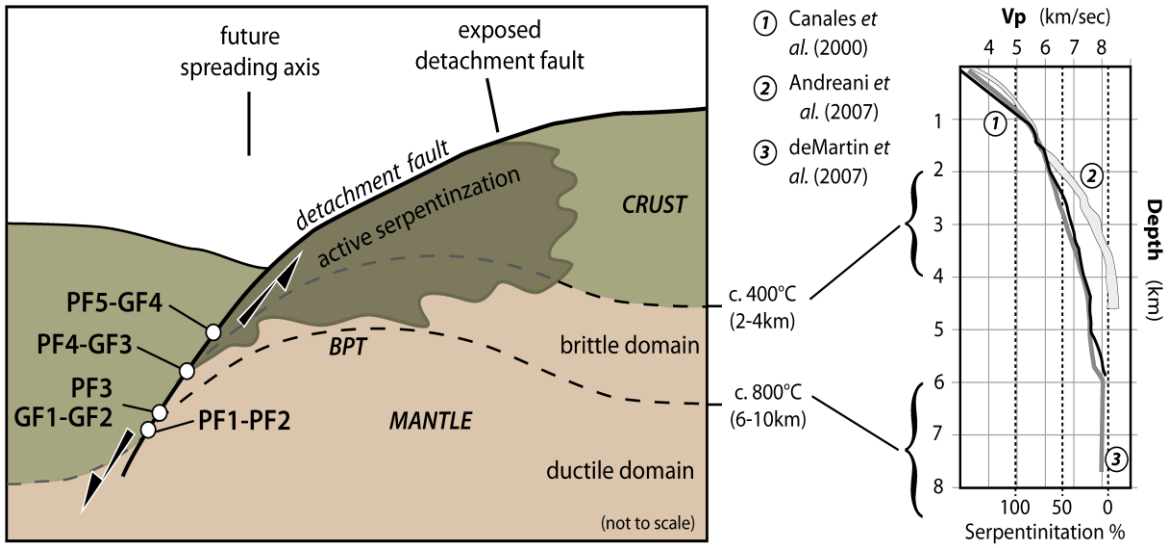

Figure 15

ACCEPTED MANUSCRIPT

ACCEPTED MANUSCRIPT

Table 1. Selected chemical analyses.

	PF1- Prototettoniti **cot 14**				PF2 tettoniti **Cot18**			PF3 myloniti **COT 16**			GF1 – **cot8** metagabbro	GF2 myl-ultramylonite **cot 9a, cot 9b**	PF4-GF3		PF5-GF4		HT-event
mineral	Ol	Opx	Sp	Cpx	Ol	Sp	Opx	Ol	Pl	OPx	Pl	Pl	Mg-Hbl	Mg-Hbl	Tr	Tr	Pl
SiO2	40.48	58.60	-	55.98	39.06	-	56.19	40.69	42.7	56.34	47.76	54.78	48.81	51.21	55.98	55.46	53.18
TiO2	-	0.02	0.11	-	-	-	0.26		-	0.04	0.00		0.53	0.57	-	0.34	0.00
Al2O3	-	0.51	28.18	0.96	-	66.35	2.68		37.2	0.88	33.15	28.57	8.25	6.11	0.96	3.00	29.47
FeO	11.56	7.25	20.52	5.10	17.39	16.1	9.75	10.81	-	6.88	0.00	0.27	5.61	6.28	5.1	3.09	0.21
MnO	0.17	0.11	0.35	0.63	0.48	0.04	0.57	0.15	bdl	0.12			0.34	0.18	0.63	0.15	0.00
MgO	48.55	31.82	11.37	22.41	43.02	17.92	27.2	49.64	bdl	35.17			22.16	24.16	22.41	24.37	0.00
CaO	0.02	0.16	-	12.13	0.03	0.07	2.28	0.14	19.62	0.16	15.50	10.45	8.75	7.57	12.13	10.43	11.18
Na2O	-	0.33	-	0.39	-	-	0.71		0.08	0.42	2.37	5.55	0.82	0.9	0.39	0.47	5.10
K2O	-	0.01	-	0.09	-	-	0.04		-	0.09	0.01	0.15	0.3	0.07	0.09	-	0.07
Cr2O3	-	-	39.59	0.11	-	-	0.06		-	0.16			-	-	-	-	0.00
total	100.7	98.81	100.1	97.8	99.98	100.48	99.74	101.43	99.6	100.26	98.79	99.77	95.67	97.1	97.8	97.31	99.38
Oxy	4	6	32	6	4	32	6	4	8	6	8	8	24	24	24	24	
Si	1.01	2.06	-	2.05	0.99	-	2.00	0.99	1.98	1.92	2.21	2.48	6.95	7.16	7.79	7.62	2.43
Ti	-	0.01	0.02	-	-	-	0.01		-	0.00	0.00	0.00	0.06	0.06	-	0.04	0.00
Al	-	0.02	8.04	0.04	-	15.84	0.11		2.04	0.03	1.81	1.52	1.39	1.01	0.21	0.49	1.58
Fe^{2+}	0.22	0.21	3.77	0.16	0.37	2.55	0.29	0.22	-	0.19	0.00	0.01	0.67	0.73	0.59	0.35	0.01
Fe^{3+}	-	-	0.38	-	-	0.18	-		-		0.00		-	-	-	-	0.00
Mn	-	0.003	0.07	0.02	0.01	0.01	0.02	0.00	-	0.00	0.00	0.00	0.04	0.02	0.07	0.02	0.00
Mg	1.76	1.67	4.10	1.22	1.63	5.41	1.44	1.79	-	1.79	0.00		4.70	5.03	4.64	4.99	0.54
Ca	0.002	0.006	-	0.48	0.00	0.02	0.09	0.00	0.98	0.00	0.77	0.51	1.34	1.13	1.81	1.54	0.45
Na	-	0.023	-	0.03	-	-	0.05		0.01	0.03	0.21	0.49	0.23	0.24	0.11	0.13	0.00
K	-	-	-	0.004	-	-	0.002		-	0.00	0.00	0.01	0.05	0.01	0.02	-	0.00
Cr	-	-	7.58	0.003	-	-	0.002		-	0.00	0.00		-	-	-	-	0.00
sum	1.98	4.01	23.97	4.00	2.02	23.99	4.00	2.03	5.00	4.05		5.01	15.41	15.41	15.11	15.17	2.73
Fo %	88.22	-	-	-	81.05	-	-	89.12	-				-	-	-	-	
En %	-	88.09	-	65.25	-	-	78.54		-	89.68			-	-	-	-	
Wo %	-	-	-	25.38	-	-	-		-	0.29			-	-	-	-	
Ab%											21.66	48.58					
An %	-	-	-	-	-	-	-		99.27		78.28	50.55	-	-	-	-	54.56

ACCEPTED MANUSCRIPT

Highlights

- the CSZ is a mylonitic shear zone affecting the Western Tethys oceanic lithosphere
- Ductile shearing occurred at temperature >800°C and continue at temperature <500°C
- It represents the deep root of an ancient analogue oceanic detachment fault
- U/Pb ages suggest that the study oceanic lithosphere is the oldest in North Apennines

ACCEPTED MANUSCRIPT